1 **Aerosol Responses to Precipitation Along North American Air Trajectories Arriving at**
2 **Bermuda**

4 Hossein Dadashazar[1], Majid Alipanah[2], Miguel Ricardo A. Hilario[3], Ewan Crosbie[4,5], Simon
5 Kirschler[6,7], Hongyu Liu[8], Richard H. Moore[4], Andrew J. Peters[9], Amy Jo Scarino[4,5], Michael
6 Shook[4], K. Lee Thornhill[4], Christiane Voigt[6,7], Hailong Wang[10], Edward Winstead[4,5], Bo
7 Zhang[8], Luke Ziemba[4], Armin Sorooshian[1,3]
8
9 [1]Department of Chemical and Environmental Engineering, University of Arizona, Tucson, AZ,
10 USA
11 [2]Department of Systems and Industrial Engineering, University of Arizona, Tucson, AZ, USA
12 [3]Department of Hydrology and Atmospheric Sciences, University of Arizona, Tucson, AZ, USA
13 [4]NASA Langley Research Center, Hampton, VA, USA
14 [5]Science Systems and Applications, Inc., Hampton, VA, USA
15 [6]Institute for Atmospheric Physics, DLR, German Aerospace Center, Oberpfaffenhofen,
16 Germany
17 [7]Institute for Atmospheric Physics, University of Mainz, Mainz, Germany
18 [8]National Institute of Aerospace, Hampton, VA, USA
19 [9]Bermuda Institute of Ocean Sciences, 17 Biological Station, St. George's, GE01, Bermuda
20 [10]Atmospheric Sciences and Global Change Division, Pacific Northwest National Laboratory,
21 Richland, WA, USA
22
23
24 *Correspondence to: Hossein Dadashazar (hosseind@arizona.edu)

Abstract

North American pollution outflow is ubiquitous over the western North Atlantic Ocean, especially in winter, making this location ~~an ideal~~a suitable natural laboratory for investigating the impact of precipitation on aerosol particles along air mass trajectories. We take advantage of observational data collected at Bermuda to seasonally assess the sensitivity of aerosol mass concentrations and volume size distributions to accumulated precipitation along trajectories (APT). The mass concentration of particulate matter with aerodynamic diameter less than 2.5 μm normalized by the enhancement of carbon monoxide above background ($PM_{2.5}/\Delta CO$) at Bermuda was used to estimate the degree of aerosol loss during transport to Bermuda. Results for December-February (DJF) show most trajectories come from North America and have the highest APTs, resulting in significant reduction (by 53%) in $PM_{2.5}/\Delta CO$ under high APT conditions (> 13.5 mm) relative to low APT conditions (< 0.9 mm). Moreover, $PM_{2.5}/\Delta CO$ was most sensitive to increases in APT up to 5 mm (-0.044 $\mu g\ m^{-3}\ ppbv^{-1}\ mm^{-1}$) and less sensitive to increases in APT over 5 mm. While anthropogenic $PM_{2.5}$ constituents (e.g., black carbon, sulfate, organic carbon) decrease with high APT, sea salt in contrast was comparable between high and low APT conditions owing to enhanced local wind and sea salt emissions in high APT conditions. The greater sensitivity of the fine mode volume concentrations (versus coarse mode) to wet scavenging is evident from AERONET volume size distribution data. A combination of GEOS-Chem model simulations of ^{210}Pb submicron aerosol tracer and its gaseous precursor ^{222}Rn reveal that (i) surface aerosol particles at Bermuda are most impacted by wet scavenging in winter/spring (due to large-scale precipitation) with a maximum in March, whereas convective scavenging plays a substantial role in summer; and (ii) North American ^{222}Rn tracer emissions contribute most to surface ^{210}Pb concentrations at Bermuda in winter (~75-80%), indicating that air masses arriving at Bermuda experience large-scale precipitation scavenging while traveling from North America. A case study flight from the ACTIVATE field campaign on 22 February 2020 reveals a significant reduction in aerosol number and volume concentrations during air mass transport off the U.S. East Coast associated with increased cloud fraction and precipitation. These results highlight the sensitivity of remote marine boundary layer aerosol characteristics to precipitation along trajectories, especially when the air mass source is continental outflow from polluted regions like the U.S. East Coast.

1. Introduction

Aerosol properties are difficult to characterize in remote marine regions owing to the scarcity of monitoring stations as compared to over land. Island observatories are critical resources to investigate long-range transport of aerosol particles and their associated properties (e.g., Silva et al., 2020). The western North Atlantic Ocean (WNAO) includes the island of Bermuda, which has a rich history of monitoring data for both surface and columnar aerosol characteristics, thus affording the opportunity to study how aerosol properties are impacted by different sources and processes along the transport of air masses to the site. Consequently, Bermuda has been the subject of decades of intense atmospheric science research (Sorooshian et al., 2020), ~~especially~~ as it is a receptor site for both North African dust (Chen and Duce, 1983) and anthropogenic outflow from both North America (Arimoto et al., 1992; Galloway et al., 1989; Moody et al., 2014; Corral et al., 2021) and Europe (Anderson et al., 1996; Cutter, 1993). North American outflow reaching Bermuda has been linked to appreciable levels of anthropogenic species (e.g., sulfate, lead, elemental carbon, ozone) (Wolff et al., 1986), more acidic rainfall as compared to other air mass sources (Jickells et al., 1982), and a significant reduction of sulfate levels in both aerosol and wet deposition samples in response to reduced SO_2 emissions in recent decades (Keene et al., 2014).

There have been extensive studies reporting on some aspect of air mass history, normally by calculating air parcel trajectories using transport and dispersion models, prior to arrival at Bermuda (Sorooshian et al., 2020 and references therein), including predominant circulation patterns impacting Bermuda at different times of the year (e.g., Miller and Harris, 1985; Veron et al., 1992). What remains uncertain is how precipitation along those trajectories impacts surface aerosol characteristics at Bermuda. Wet scavenging rates are very difficult to constrain over open ocean areas such as the WNAO (Kadko and Prospero, 2011~~).~~) not only because of complexity of physical mechanisms in play but also scarce necessary field measurements. Overall, more work is warranted to better constrain wet scavenging of aerosol particles along trajectories as such studies are sparse not only for the WNAO but also for other regions (Tunved et al., 2013; Hilario et al., 2021). Arimoto et al. (1999) used aerosol radionuclide data in relation to airflow pattern information to conclude that pollutant transport to Bermuda is common from the northwest and that precipitation scavenging can be influential; their analysis of rain effects on nuclide activities were based on rain data collected at Bermuda without knowledge of ~~rain along trajectory pathways.~~precipitation transport history prior to arrival. While many studies have investigated how composition at Bermuda varies based on air mass trajectories~~,~~ (Miller and Harris, 1985; Cutter, 1993; Huang et al., 1996), the subject of how precipitation along those trajectories impact the resultant aerosol at Bermuda has not been adequately addressed but is motivated by past works (Moody and Galloway, 1988; Todd et al., 2003).

In their recent aerosol climatology study for Bermuda, Aldhaif et al. (2021) found the peculiar result that fine particulate pollution in the winter months (December-February) was reduced even though there was an enhanced number density of air mass back trajectories traced back to North America. They hypothesized that enhanced seasonal cloud fractions and precipitation in winter (Painemal et al., 2021) contribute to the removal of aerosol particles during transport via wet scavenging, which we aim to study more deeply here using a variety of datasets. Results of this study have broad relevance to all remote marine regions impacted by transported continental pollution, in addition to advancing knowledge of how precipitation can impact surface aerosol characteristics.

2. Datasets and Methods

103   Datasets used in this work are summarized in Table 1 and described in brief detail below.
104
105
106
107
108
109 **Table 1. Summary of datasets used in this work. Data are between 1 January 2015 and 31**
110 **December 2019, with the exception of ACTIVATE aircraft data based on a single flight day**
111 **on 22 February 2020.** ~~GEOS-Chem simulations are separately described in Section 2.5.~~
112 **Section 2 provides more details about the datasets used in this study, including specific**
113 **instruments from the ACTIVATE airborne dataset.**
114
115

Parameter	Acronym	Data Source	Time Resolution	Website
~~Particulate matter mass concentration (aerodynamic diameter less than 2.5 µm)~~	~~PM$_{2.5}$~~	~~Fort Prospect Station~~	~~Hourly~~	~~https://doi.org/10.6084/m9.figshare.13651454.v2~~
~~Particulate matter mass concentration (aerodynamic diameter less than 10 µm)~~	~~PM$_{10}$~~	~~Fort Prospect Station~~	~~Daily~~	~~https://doi.org/10.6084/m9.figshare.13651454.v2~~
~~Nitrogen monoxide concentration~~	~~NO~~	~~Fort Prospect Station~~	~~Hourly~~	~~https://doi.org/10.6084/m9.figshare.13651454.v2~~
~~Nitrogen dioxide concentration~~	~~NO$_2$~~	~~Fort Prospect Station~~	~~Hourly~~	~~https://doi.org/10.6084/m9.figshare.13651454.v2~~
~~Nitrogen oxide concentration~~	~~NO$_x$~~	~~Fort Prospect Station~~	~~Hourly~~	~~https://doi.org/10.6084/m9.figshare.13651454.v2~~
~~Volume size distribution~~	~~VSD~~	~~AERONET~~	~~Hourly~~	~~https://aeronet.gsfc.nasa.gov/~~
~~Carbon monoxide surface concentration~~	~~CO~~	~~MERRA-2~~	~~Hourly~~	~~https://disc.gsfc.nasa.gov/~~
~~Aerosol speciated surface mass concentrations~~	~~-~~	~~MERRA-2~~	~~Hourly~~	~~https://disc.gsfc.nasa.gov/~~
~~Surface wind speed~~	~~Winds$_F$~~	~~MERRA-2~~	~~Hourly~~	~~https://disc.gsfc.nasa.gov/~~
~~Planetary boundary layer height~~	~~PBLH~~	~~MERRA-2~~	~~Hourly~~	~~https://disc.gsfc.nasa.gov/~~
~~Back-trajectory~~	~~-~~	~~HYSPLIT~~	~~N/A~~	~~https://www.ready.noaa.gov/HYSPLIT.php~~
~~Precipitation~~	~~APT/Rain~~	~~GDAS~~	~~Hourly~~	~~https://www.ready.noaa.gov/archives.php~~
~~Aerosol/cloud properties~~	~~-~~	~~Airborne: ACTIVATE~~	~~1 – 45 Sec~~	~~https://doi.org/10.5067/SUBORBITAL/ACTIVATE/DATA001~~

116
117
118

Parameter	Acronym	Data Source	Spatial Resolution	Time Resolution
Particulate matter mass concentration (aerodynamic diameter less than 2.5 µm)	PM$_{2.5}$	Fort Prospect Station	-	Hourly
Particulate matter mass concentration (aerodynamic diameter less than 10 µm)	PM$_{10}$	Fort Prospect Station	-	Daily
Nitrogen monoxide concentration	NO	Fort Prospect Station	-	Hourly
Nitrogen dioxide concentration	NO$_2$	Fort Prospect Station	-	Hourly
Nitrogen oxide concentration	NO$_x$	Fort Prospect Station	-	Hourly
Volume size distribution	VSD	AERONET	-	Hourly
Carbon monoxide surface concentration	CO	MERRA-2	0.625° × 0.5°	Hourly
Aerosol speciated surface mass concentrations	-	MERRA-2	0.625° × 0.5°	Hourly
Surface wind speed	Winds$_F$	MERRA-2	0.625° × 0.5°	Hourly
Planetary boundary layer height	PBLH	MERRA-2	0.625° × 0.5°	Hourly
Precipitation	APT/Rain	GDAS	1° × 1°	Hourly

| Aerosol/cloud properties | - | Airborne: ACTIVATE | - | 1 – 45 Sec |

2.1 Bermuda Surface Measurements

Aerosol and gas measurements were conducted at Fort Prospect in Bermuda (32.30° N, 64.77°W, 63 m ASL). Hourly $PM_{2.5}$ data were collected with a Thermo Scientific TEOM 1400a Ambient Particulate Monitor with 8500C FDMS (Federal Equivalent Method EQPM-0609-181 for $PM_{2.5}$). Concentrations were determined by employing conditioned filter sample collection and direct mass measurements using an inertial micro-balance (TEOM 1400a). Hourly precision was ± 1.5 µg m^{-3}. Hourly data were averaged ~~every~~over 6 ~~hours~~hour intervals to match the time frequency of the trajectory ~~analysis~~data discussed subsequently. The conversion of hourly data to 6 hour data also helps to mask, to some extent, the unwanted effects of local sources and processes that occur on a small timescale.

PM_{10} concentrations were determined based on U.S. Environmental Protection Agency (EPA) method IO-2 (EPA, 1999) using a Tisch model TE6070 hi-volume air sampler, equipped with 8" × 10" TissuQuartz 2500 QAT-UP quartz fiber filters. The PM_{10} sampler was operated at a flow rate of 2.1 m^3 min^{-1} yielding a total volume of 3000 m^3 over a 24 hr sampling period. The sampler flow rate was calibrated every 3 months. Sampling was synchronized with the 1-in-6 day national ambient air quality schedule used by EPA. Prior to deployment, the filters were equilibrated for 24 hr in an environmental control chamber maintaining constant conditions of relative humidity ($35 \pm 2\%$) and temperature ($21 \pm 2°C$). The filters were then weighed with a precision of ± 0.1 mg using a Mettler Toledo AB104 balance, which was modified for weighing unfolded 8" × 10" filters, and then transferred to clean re-sealable plastic bags for transportation to the field site. After sampling, the exposed filters were returned immediately to the laboratory where they were re-equilibrated in the environmental control chamber for 24 hr before being re-weighed to determine the particle loading from which particle concentrations were calculated. PM_{10} determinations have an accuracy of within $\pm 2.5\%$, which is equivalent to ± 0.2 µg m^{-3} based on the average of $PM_{2.5}$ between 2015 and 2019 (i.e., 6.7 µg m^{-3}).

Various gases were monitored with hourly time resolution using a Model T200U Trace-level $NO/NO_2/NO_x$ analyzer (Teledyne API), which is a U.S. EPA compliance analyzer relying on a proven chemiluminescence principle. The gas analyzer was routinely calibrated using NIST-certified calibrant NO_2 in ultra-high purity nitrogen (Airgas, Inc., Radnor Township, PA, USA). Acceptable criteria applied for single point quality control (QC) allows for $\pm15.1\%$ or $< \pm1.5$ ppb difference, whichever is greater (40 CFR Part 58 App A Sec. 3.1.1). Similar to $PM_{2.5}$, these hourly gas data were averaged to 6-hour resolution.

There were a few periods when data were missing with the longest one being between 11 January 2016 and 08 April 2016 for the gases, and also between 16 October 2017 and 20 January 2018 for $PM_{2.5}$. There was no major discontinuity in PM_{10} sampling. Table S1 reports the number of data points available for various seasons from the surface measurements at Fort Prospect in Bermuda.

Columnar aerosol data were obtained from a NASA AErosol RObotic NETwork (AERONET) (Holben et al., 1998) surface station at Tudor Hill (32.264° N, 64.879° W). Level 2 daily data have been quality assured and cloud screened based on the Version 3 algorithm (Giles et al., 2019). We focus on the volume size distribution (VSD) product that has 22 logarithmically equidistant discrete radii ranging from 0.05 to 15 µm. A radius of 0.6 µm typically discriminates

163 between fine and coarse modes when using AERONET data (Dubovik et al., 2002; Schuster et al.,
164 2006).
165
166 **2.2 Reanalysis Data**
167   Modern-Era Retrospective analysis for Research and Applications-Version 2 (MERRA-2)
168 (Gelaro et al., 2017) products were used as a data source for speciated aerosol and gas parameters
169 including surface mass concentration of sea-salt (collection "tavg1_2d_aer_Nx") and surface
170 concentration of carbon monoxide (CO; collection "tavg1_2d_chm_Nx"). Surface wind speed and
171 planetary boundary layer height (PBLH) (collection "tavg1_2d_flx_Nx") data were also obtained
172 from MERRA-2. Hourly and 3-hourly data were downloaded and averaged for a 0.5° latitude by
173 0.625° longitude grid (i.e., 32° – 32.5°N and 64.375° – 65°W) surrounding Bermuda and
174 subsequently converted toaveraged over 6-hour dataintervals to match the time frequency of
175 trajectory analysis results. It should be noted that MERRA-2 data were temporally and spatially
176 coincident with the ending point of trajectories over Bermuda. The Global Data Assimilation
177 System (GDAS) one-degree archive data were used for trajectory calculations explained in the
178 subsequent section. Precipitation data were also obtained along the trajectories based on GDAS
179 one-degree data.
180
181 **2.3 Air Mass Trajectory Analysis**
182   To track air mass pathways arriving at Bermuda (32.30° N, 64.77°W), we obtained 10-day
183 (240 hr) back-trajectories from the Hybrid Single-Particle Lagrangian Integrated Trajectory model
184 (HYSPLIT) (Stein et al., 2015; Rolph et al., 2017). We used an ending altitude of 100 m (AGL) to
185 be within the surface layer and close to the measurement site. As discussed later, sensitivity
186 analysis with higher ending altitudes (500 m and 1 km; Figs. S1-S2) revealreveals similar results
187 to using 100 m. Four trajectories were initialized (i.e., 6-hour interval) each day between 1 January
188 2015 00:00:00 UTC and 31 December 2019 18:00:00 UTC resulting in a total of 7304 individual
189 trajectories. Trajectories were calculated using the Global Data Assimilation System (GDAS) one-
190 degree archive data and with the "model vertical velocity" method, which is a way that means
191 vertical motion ismotions were handled in HYSPLIT for trajectory calculations.
192 Precipitationdirectly using meteorological data were also obtainedfiles. Moreover, accumulated
193 precipitation along the trajectories based on(APT) was calculated by integrating surface
194 precipitation data from GDAS one-degree datathroughout the transport to the receptor site. As
195 GDAS precipitation data corresponds to the surface level, it should be noted that APT values
196 presented in this study are associated with the potential maximum level of precipitation
197 experienced by the air parcel through its transport journey. Results presented in Figs. 1-3 are based
198 on 10-day back-trajectories, whereas analyses presented in the remaining sections of the paper are
199 based on 4-day (96 hr) back-trajectories.
200   Trajectory analyses contain errors that originate from factors including, but not limited to,
201 the choice of input meteorological data, resolution of input data, and the vertical transport method
202 used in trajectory calculations (Stohl et al., 1995; Cabello et al., 2008; Engström and Magnusson
203 2009). Although the choice of meteorological data is the most important contributor to the
204 uncertainties associated with trajectories calculations (Gebhart et al., 2005), no particular dataset
205 has been found to be superior in terms of yielding the lowest error. While in this study we used
206 GDAS data, which have been widely used as input dataset for trajectory calculations even in
207 regions with complicated topography (e.g., Tunved et al., 2013; Su et al., 2015), the
208 aforementioned inherent errors should not be overlooked when interpreting the results presented

in this work. Another factor that can contribute to the uncertainties for the results presented in this work is the use of GDAS as the source of precipitation data as previous works (Sun et al., 2018; Nogueira 2020) have demonstrated that there is some level of disagreement between precipitation datasets.

2.3.1 Concentration Weighted Trajectory Analysis and Seasonal Rain Maps

Concentration weighted trajectories (CWT) were calculated based on the 10-day back-trajectories from HYSPLIT in conjunction with Bermuda surface $PM_{2.5}$ data described in Section 2.1. The CWT method has been implemented widely to identify long-range pollutant transport pathways impacting a receptor site (Hsu et al., 2003; Wang et al., 2009; Hilario et al., 2020). Seasonal maps of average precipitation experienced by trajectories were also estimated based on 10-day back-trajectories from HYSPLIT. The aforementioned analyses were performed for $0.5°×0.5°$ grids covering the area encompassed by $10°–80°N$ and $5°–170°W$. A weight function (W_{ij} in Eq. 1) following the method of Dimitriou et al. (2015) was applied in the CWT analysis and precipitation maps to increase statistical stability. In Eq. 1, n_{avg} is the average number of trajectory end points per individual gird cell over the study region excluding cells with zero trajectory points and n_{ij} is the number of trajectory end points that lies in the grid cell (i,j).

$$W_{ij} = \begin{cases} 1 & n_{ij} > 3\,n_{avg} \\ 0.7 & 1.5\,n_{avg} < n_{ij} < 3\,n_{avg} \\ 0.4 & n_{avg} < n_{ij} < 1.5\,n_{avg} \\ 0.2 & n_{ij} < n_{avg} \end{cases} \qquad (1)$$

10-day back trajectories were implemented for generating CWT and rain maps to illustrate potential distant sources impacting Bermuda. But for more quantitative analyses presented in the subsequent sections focused on transport most relevant to the WNAO region, four-day back trajectories were used by simply truncating 10-day trajectories. The use of four-day trajectories reduces the uncertainties associated with trajectory calculations in comparison to using 10-day trajectories and also enables us to focus on sources closer to the receptor site.

2.3.2 Trajectory Clustering

Hierarchical agglomerative clustering was used to identify characteristic trajectories reaching Bermuda at 100 m (AGL). Hierarchical clustering was based on the "complete linkage" method (Govender and Sivakumar, 2020). Four-day HYSPLIT back-trajectories were used to perform clustering analysis. Distances between trajectories were calculated using the Haversine formula, which calculates distance between two points on Earth assuming they are on a great circle (Sinnott, 1984). The distance between any two trajectories was calculated as the sum of distances between trajectory endpoints. Subsequently, clustering was conducted based on the symmetric distance matrix, which includes the distances between all pairs of trajectories. Clustering was performed for varying numbers of clusters, ranging between 2 and 32. The L-method (Kassomenos et al., 2010) was implemented to identify the optimum number of clusters. In this method, root mean square deviation (RMSD) was calculated for each clustering run and then plotted versus the

254 number of clusters to determine the optimum solution. RMSDs were estimated based on the
255 distances between trajectories and associated mean cluster trajectories.
256
257 **2.4 Airborne Measurements**
258   Airborne data from the Aerosol Cloud meteorology Interactions oVer the western ATlantic
259 Experiment (ACTIVATE) are used from Research Flight 6 (RF6) on 22 February 2020.
260 ACTIVATE involves two NASA Langley aircraft (HU-25 Falcon and UC-12 King Air) flying in
261 coordination at different altitudes to simultaneously characterize the same vertical column with a
262 focus on aerosol-cloud-meteorology interactions (Sorooshian et al., 2019). RF6 was a rare case of
263 the HU-25 Falcon flying alone, but this aircraft conveniently included measurements relevant to
264 this study. The ACTIVATE strategy involves the HU-25 Falcon flying in the boundary layer to
265 characterize gas, aerosol, cloud, and meteorological parameters along the following level legs:
266 Min. Alt. = lowest altitude flown (500 ft), BCB = below cloud base, ACB = above cloud base,
267 BCT = below cloud top, ACT = above cloud top.
268   Data from the following instruments were used: Condensation Particle Counter (CPC; TSI
269 Model 3772) for number concentration of particles with diameter > 10 nm; Scanning Mobility
270 Particle Sizer (SMPS; TSI Model 3081) for aerosol size distribution data between 3.2 – 89.1 nm;
271 Laser Aerosol Spectrometer (LAS; TSI Model 3340) for aerosol size distribution data between
272 diameters of 0.09 – 5 µm; two-dimensional optical array imaging probe (2DS; SPEC Inc.) (Lawson
273 et al., 2006) for rain water content (RWC) quantified by integrating rain drop size distributions
274 between diameters of 39.9 – 1464.9 µm; and Fast Cloud Droplet Probe (FCDP; SPEC Inc.) (Knop
275 et al., 2021) for cloud liquid water content (LWC) calculated by integrating drop size distributions
276 between diameters of 3 – 50 µm. With the exception of SMPS data (45 second resolution), all
277 airborne data were at 1 second resolution.
278
279 **2.5 Radionuclide tracers in GEOS-Chem Model**
280   Lead-210 (^{210}Pb, half-life 22.3 years) is the decay daughter of ~~Radon-222 (^{222}Rn~~(, half-life
281 3.8 days) emitted mainly from land surfaces. After production, it indiscriminately attaches to
282 ambient submicron particles, which move with the air until being scavenged by precipitation or
283 deposited to the surface. Because of its relatively well-known source and wet deposition as its
284 principal sink, ^{210}Pb has long been used to test wet deposition processes in global models (e.g., Liu
285 et al., 2001). It is also a useful tracer to describe continental air influence over oceans. In this study,
286 we use ^{210}Pb as simulated by the ~~GOES~~GEOS-Chem model to investigate the role of precipitation
287 scavenging in affecting seasonal surface aerosol concentrations at Bermuda.
288   GEOS-Chem (http://www.geos-chem.org) is a global 3-D chemical transport model driven
289 by meteorological fields from the Goddard Earth Observing System (GEOS) of the NASA Global
290 Modeling and Assimilation Office (Bey et al., 2001; Eastham et al., 2014). It has been widely used
291 to study trace gases and aerosols in the atmosphere. Here we use the model version 11-01
292 (http://wiki.seas.harvard.edu/geos-chem/index.php/GEOS-Chem_v11-01) driven by the MERRA-
293 2 reanalysis (at 2.5° longitude by 2° latitude resolution) to simulate ^{222}Rn and ^{210}Pb. The model
294 simulates the emission, transport (advection, convection, boundary layer mixing), deposition, and
295 decay of the radionuclide tracers (Liu et al., 2001; Brattich et al., 2017; Yu et al., 2018; Zhang et
296 al., 2021). As a function of latitude, longitude, and month, ^{222}Rn emission uses a customized
297 emission scenario that was built upon previous estimates and evaluated against global ^{222}Rn
298 surface observations and vertical profile measurements (Zhang et al., 2021). GEOS-Chem uses the
299 TPCORE advection algorithm of Lin and Rood (1996), calculates convective transport using

300   archived convective mass fluxes (Wu et al., 2007), and uses the non-local boundary-layer mixing
301   scheme implemented by Lin and McElroy (2010). The wet deposition scheme follows that of Liu
302   et al. (2001) and includes rainout (in-cloud scavenging) due to large-scale (stratiform and anvil)
303   precipitation, scavenging in convective updrafts, and washout (below-cloud scavenging) by
304   precipitation (Wang et al., 2011). A modification to the large-scale precipitation scavenging
305   scheme is included to use spatiotemporally varying cloud water contents from MERRA-2 instead
306   of a fixed constant value in the original model (Luo et al., 2019). Dry deposition is based on the
307   resistance-in-series scheme of Wesely (1989).
308
309   **3. Results and Discussion**
310   **3.1 Seasonal Profiles**
311   **3.1.1 Back-Trajectories**
312   Our results in Fig. 1 show that the summer months (June-August, JJA) are distinct due to
313   the Bermuda High promoting easterly winds at latitudes south of Bermuda that turn north and
314   become southwesterly (~ parallel to U.S. East Coast) towards Bermuda. The Bermuda high
315   pressure system and its associated anticyclonic circulation in the boundary layer have been
316   reported to be strongest in April–September (Merrill, 1994; Moody et al., 1995). This high pressure
317   system breaks down in other months in favor of strengthened extratropical subpolar low pressure,
318   thus yielding more air influence from the northwest and west (Arimoto et al., 1995; Davis et al.,
319   1997), which is clearly evident in the other three seasonal panels of Fig. 1 and most pronounced
320   in the winter months (December-February, DJF). In their analysis of air mass history leading to
321   rain events over Bermuda, Altieri et al. (2013) observed more influence from air originating over
322   water in warmer months (April–September) and faster moving air masses originating over the
323   continental U.S. primarily in the colder months of October–March. Moody and Galloway (1988)
324   also showed that cool months (October–March) were marked by more transport from the U.S. East
325   Coast. It can be deduced from Fig. 1 that based on the farther reaching source areas of the back-
326   trajectories in colder months, and especially DJF, that air moves faster in the boreal winter. Finally,
327   we note that Figs. S1-S2 show the same results as Fig. 1 but with ending altitudes of 500 m and 1
328   km over Bermuda; the sensitivity tests indicate the same general results and thus we continue the
329   discussion using results based on 100 m.
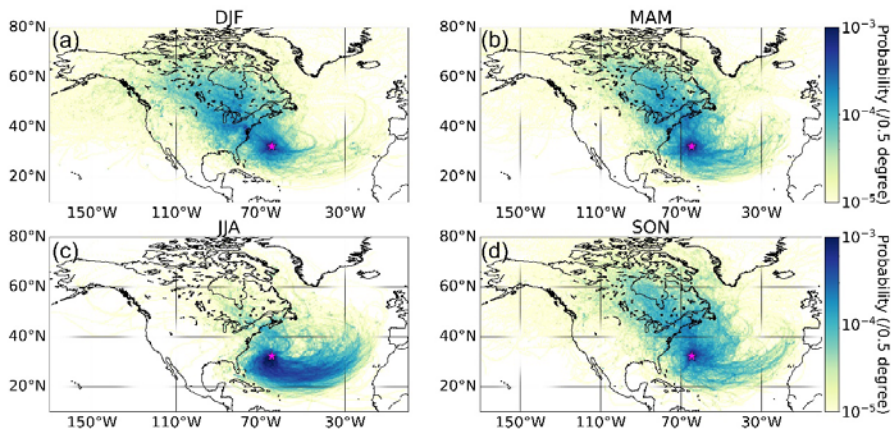
330
331 **Figure 1. Seasonal maps (a-d) showing the probability density of trajectories calculated**
332 **based on 10-day HYSPLIT backward trajectories reaching Bermuda (32.30° N, 64.77°W),**
333 **denoted by the pink star, at 100 m (AGL). This analysis is based on trajectories between 01**
334 **January 2015 and 31 December 2019. Analogous results for ending altitudes of 500 m and 1**
335 **km are shown in Figs. S1 and S2, respectively.**

336
337 **3.1.2 Surface Aerosol and NO$_x$**
338   Recent work has shown a seasonal cycle over Bermuda for column-integrated aerosol
339 properties, with aerosol optical depth (AOD) being highest in March-May (MAM) and JJA and
340 lowest in September-November (SON) and DJF (Aldhaif et al., 2021). They further showed that
341 sea salt contributed more to AOD in the colder months (SON, DJF) whereas sulfate, organic
342 carbon, black carbon and dust were more dominant in MAM and JJA. In their examination of
343 aerosol type seasonality at Bermuda, Huang et al. (1999) observed that marine and crustal elements
344 peaked in winter and summer, respectively, and that pollution-derived particles dominated in
345 spring with a smaller peak in fall. We use data from Fort Prospect ~~datastation~~ to gain a revised
346 perspective about seasonality and the weekly cycle of surface layer aerosol and additionally NO$_x$
347 (box notch plots in Figs. S3a-f).
348   Median seasonal concentrations of PM$_{2.5}$ (μg m^{-3}) were as follows at Bermuda, being
349 largely consistent with the AOD seasonal cycle: DJF = 5.50, MAM = 6.36, JJA = 6.11, SON =
350 5.33 (Fig. S3). NO$_x$ exhibited a similar seasonal pattern (ppbv): DJF = 17.76, MAM = 21.62, JJA
351 = 18.68, SON = 13.95 (Fig. S3). It is difficult to ascertain sources and impacts of precipitation on
352 PM$_{2.5}$ based on these values. As a next step we present the seasonal CWT maps showing the
353 predominant pathways accounting for the majority of PM$_{2.5}$ at Bermuda (Fig. 2). Expectedly, PM$_{2.5}$
354 in JJA is largely accounted for by trajectories following the general anticyclonic circulation already
355 shown in Fig. 1c associated with the Bermuda High. These air masses are enriched with African
356 dust as has been documented in many past studies (e.g., Arimoto, 2001; Huang et al., 1999; Muhs
357 et al., 2012). In contrast, the other seasons (especially DJF and MAM) showed greater relative
358 influence from North American outflow versus other source regions.

Formatted: Font color: Auto	
Formatted: Font color: Auto	
Formatted: Font color: Auto	
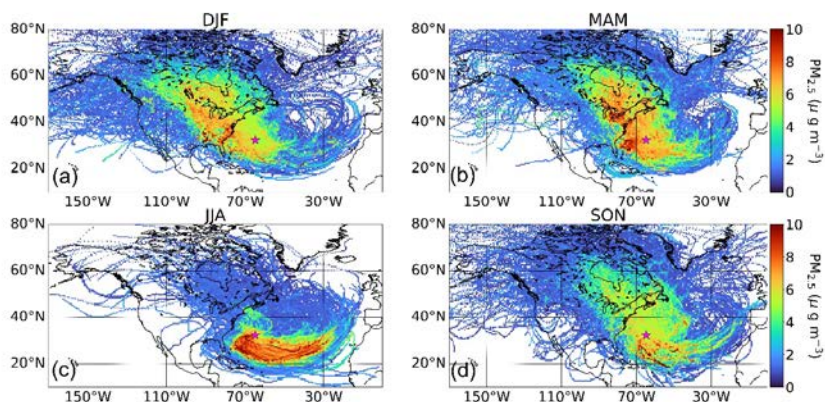
Figure 2. Seasonal (a-d) concentration-weighted trajectory maps (CWT) for PM₂.₅ measured at Fort Prospect in Bermuda, denoted by the pink star. This analysis is based on trajectories between 1 January 2015 and 31 December 2019.

While we focus on long-range transport of $PM_{2.5}$ to Bermuda, local sources cannot be ignored, including both sea salt and non-sea salt species (e.g., Galloway et al., 1988). The island has a population of approximately 64,000 as of 2016 (Government of Bermuda, 2019). Local influence from anthropogenic sources has been reported to be insignificant in contrast to transported pollution (Galloway et al., 1988; Keene et al., 2014). We assess how significant local anthropogenic sources are based on day-of-week aerosol concentrations and whether significantly higher levels exist on working days as compared to weekend days as shown in other regions with strong anthropogenic influence (Hilario et al., 2020 and references therein). Our analysis found negligible difference between working days (Monday-Friday) and weekend days (Saturday-Sunday) for both $PM_{2.5}$ and NO_x when analysis was done based on annual (Figs. S3b/d), including when resolved by season) or seasonal data (Figs. S4-S5). Therefore, it is less likely that local anthropogenic emissions dominate the island's $PM_{2.5}$ and NO_x, providing support for transported sources being more influential; as will be shown, normalizing $PM_{2.5}$ by CO helps control for local anthropogenic influence.

We also examined seasonal and day-of-week statistics for PM_{10} to assess the relative importance of coarse aerosol types including mainly sea salt and dust (Figs. S3e-f). Results reveal the highest median PM_{10} values ($\mu g\ m^{-3}$) in DJF (19.24), followed by MAM (18.51), JJA (17.98), and SON (15.88). As will be shown later and already documented (Aldhaif et al., 2021), surface wind speeds around Bermuda are highest in DJF, contributing to higher sea salt emissions. Expectedly there was no observable PM_{10} weekly cycle as dust and sea salt are naturally emitted. Both $PM_{2.5}$ and PM_{10} exhibited their highest seasonal standard deviations in JJA owing most likely to the episodic nature of some pollution events such as with dust and biomass burning (e.g., Aldhaif et al., 2021).

3.1.3 Precipitation Along Trajectories

389   Figure 3 shows seasonal profiles of average precipitation rate obtained from GDAS (Table
390   1) in 0.5°×0.5° grids based on 10-day back trajectories arriving at Bermuda (100 m AGL). The
391   spatiotemporal pattern of precipitation over the WNAO is of most interest in terms of potential
392   impacts on wet scavenging of aerosol during the transport of North American pollution to
393   Bermuda. In that regard, DJF shows the most pronounced levels of precipitation to the north and
394   northwest of Bermuda over the WNAO, coincident with strong and frequent convection linked to
395   frontogenesis (Painemal et al., 2021). This is consistent with how Painemal et al. (2021) showed
396   that precipitation exhibits maximum levels over the Gulf Stream path owing to relatively high sea
397   surface temperature and strong surface turbulent fluxes.
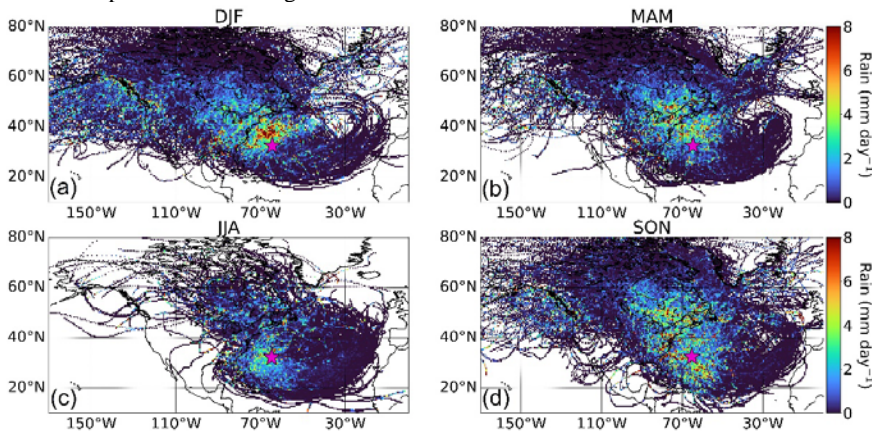
398
399   **Figure 3. Seasonal maps (a-d) of average precipitation occurring in 0.5°×0.5° grids based on**
400   **10-day backward trajectories reaching Bermuda (32.30° N, 64.77°W; pink star) at 100 m**
401   **(AGL). This analysis is based on trajectories between 1 January 2015 and 31 December 2019.**
402
403   **3.2 Trajectory Clustering**
404   Prior to examining how precipitation directly impacts $PM_{2.5}$ at Bermuda, we identify
405   characteristic trajectory pathways using the hierarchical agglomerative clustering method
406   described in Section 2.3.2. We reiterate that this analysis is based on 4 days of back-trajectories,
407   rather than 10 days from Figs. 1-3, to focus more on transport closer to Bermuda. The optimum
408   solution based on the L-method (see Section 2.3.2) resulted in eight trajectory clusters (Fig. 4a),
409   with five (numbered 1-5) coming from North America and the remaining three (numbered 6-8)
410   more characteristic of the anticyclonic circulation described already for JJA. The former five
411   clusters account for 49% of the total trajectories, with the latter three responsible for the remaining
412   51%. The majority of trajectories from North America come offshore north of North Carolina (i.e.,
413   coastal areas north of ~35°N) .
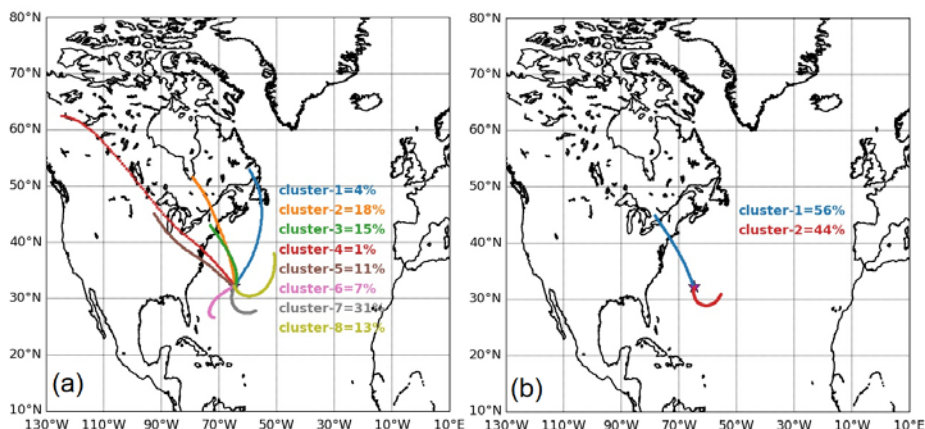
414
415 **Figure 4. Cluster mean trajectories based on the (a) optimum solution having eight clusters**
416 **and (b) a simplified solution with two clusters to enhance statistics for North American**
417 **trajectories. Clustering was performed on four-day HYSPLIT backward trajectories**
418 **between 1 January 2015 and 31 December 2019.**
419
420   For the sake of simplicity of the remainder of the discussion, we reduced the number of
421 characteristic trajectories to two (Fig. ~~4b)~~4b), by conducting a new clustering analysis, to have one
422 from North America and the other from the southeast. Using only two clusters increases the
423 number of data points in the North American cluster for more robust calculations of rain-aerosol
424 relationships. Our choice to put together all North American air mass clusters into one group is
425 aligned with a similar clustering choice by Chen and Duce (1983; see their Fig. 3) where
426 trajectories were grouped together from Florida to the Canadian maritime provinces. Also, Mead
427 et al. (2013) divided trajectory data ending at Bermuda into "Saharan" and "non-Saharan" seasons
428 that generally coincide with our division of data into two clusters. Cluster 1 from North America
429 accounts for 56% of trajectories and Cluster 2 from the southeast is linked to 44% of trajectories.
430 It is clear from the two clusters that the North American air masses generally move faster as the
431 characteristic 4-day back-trajectories originate farther away from Bermuda than that of Cluster 2.
432   Regardless of season, Cluster 1 was associated with higher APT values with the seasonal
433 median values (units of mm) as follows (Cluster1/Cluster 2): DJF = 6.1/2.3; MAM = 5.2/1.8; JJA
434 = 6.7/2.8; SON = 7.0/5.1. Figure 5 shows a box notch plot comparing APT between clusters for
435 each season, demonstrating statistically significant differences in median values between clusters
436 for a given season at 95% confidence. Furthermore, Cluster 1 exhibited higher CO levels at
437 Bermuda for each season with median values (units of ppbv) as follows (Cluster 1/Cluster 2): DJF
438 =89.7/76.3; MAM = 88.5/75.0; JJA = 68.9/58.7; SON = 81.6/65.6. Therefore, the combination of
439 pollution outflow from North America and higher APT values makes Cluster 1 more ~~ideal~~relevant
440 in terms of identifying potential wet scavenging effects on transported aerosol over the WNAO.
441 The remainder of the study thus focuses on Cluster 1.

442

443
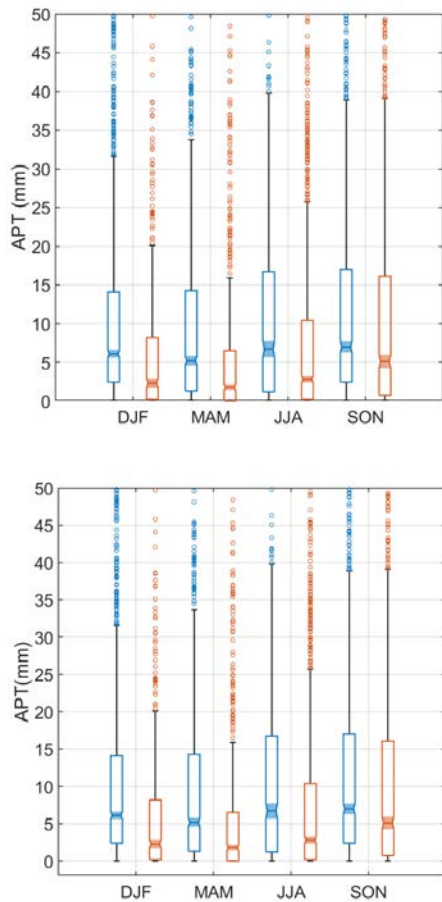
Figure 5. Box notch plot for each season comparing accumulated precipitation along trajectories (APT) for Clusters 1 (blue) and 2 (orange) from Fig. 4b. APT values were estimated from four-day HYSPLIT back trajectories reaching Bermuda (32.30° N, 64.77°W) at 100 m AGL. The middle, bottom, and top lines in each box represent the median, 25th percentile, and 75th percentile, respectively. Markers show extreme values identified based on 1.5×IQR (interquartile range) distance from the top of each box. Whiskers represent maximum and minimum values excluding extreme points. Boxes with notches and shaded regions that do not overlap have different medians at the 95% confidence level.

3.3 North America Trajectory Results

We next examine the relationship between APT and aerosol transport to Bermuda based on Cluster 1 results (Table 2). We compare data for "low" and "high" APT values based on

thresholds being the 25th percentile (< 0.9 mm) and 75th percentile (> 13.5 mm), respectively, based on cumulative data from all seasons and years. As wet scavenging is expected to reduce $PM_{2.5}$ during its transport from North America to Bermuda, we anticipate lower $PM_{2.5}$ values at high APT. However, the results indicate this is only the case for MAM and JJA, with similar median values in SON and a higher median value in DJF for high APT conditions. Interestingly, NO, NO_2, NO_x, and CO were all significantly higher in DJF for high APT conditions too~~, raising~~. This raises the issue that absolute $PM_{2.5}$ concentrations should be normalized to account for the differences in concentration that existed closer to North America prior to potential wet scavenging over the WNAO.

To study the effects of wet removal processes on aerosol particles during long-range transport to a receptor site, many studies have used aerosol concentrations normalized by the concentration of an inert gaseous species co-emitted with particles at distance sources. Such normalization is critical and superior to the use of only aerosol concentration as the latter can be influenced by local sources that can mask aerosol response to removal processes during long-range transport. CO exhibits three important traits qualifying it as a species to normalize $PM_{2.5}$ by: (i) a reliable marker of anthropogenic pollution stemming from North America (Corral et al., 2021); (ii) being relatively insensitive to wet scavenging processes; and (iii) having a long lifetime in the atmosphere (~1 month; Weinstock, 1969) compared to aerosol particles. Consequently, we normalize $PM_{2.5}$ by ΔCO to quantify transport efficiency and to reveal the potential effects of wet scavenging as has been done in past studies for other regions (Park et al., 2005; Garrett et al., 2010; Hilario et al., 2021; Matsui et al., 2011; Moteki et al., 2012; Oshima et al., 2012). We first determine the 5th percentile value of surface CO at Bermuda for each season for Cluster 1 trajectories and assume those are the seasonal background values as done also by Matsui et al. (2011). We then calculate ΔCO as the difference between each 6-hourly CO data point at Bermuda and the background value for a given season. We only use data when $\Delta CO > 3.2$ ppbv to ensure a sufficiently high signal to noise ratio (Garrett et al., 2010).

Table 2. Seasonal medians of aerosol, gas, and meteorological variables for Cluster 1 divided into high- and low-APT categories. Differences in median values that are statistically significant (p-value < 0.05) based on a Wilcoxon rank-sum test are highlighted with bold and italic font. Percentage differences[*] between high- and low-APT median values are provided in parentheses. NO, NO_2, NO_x, and $PM_{2.5}$ are based on Fort Prospect measurements, whereas all other parameters are from MERRA-2 with the exception of the two APT rows (derived from HYSPLIT and GDAS) and the last 8 rows corresponding to AERONET volume size distribution data. We combined all seasons for AERONET data to have sufficient statistics for comparisons (high APT = 16 points, low APT = 19 points). AERONET parameters include volume concentration (V), effective radii (R_{eff}), volume median radii (R), and geometric standard deviation (σ) with subscripts f and c for fine and coarse modes, respectively. Number of data points for each table entry is summarized in Table ~~S1~~S2.

496

	High-rain (APT > 13.5 mm)/Low-rain (APT < 0.9 mm) (% Difference[*])			
Parameter	DJF	MAM	JJA	SON
NO (ppbv)	*6.0/3.5 (71 %)*	7.3/7.8 (-6 %)	*8.3/13.1 (-37 %)*	3.8/4.2 (-10 %)
NO$_2$ (ppbv)	*13.9/12.8 (9 %)*	13.4/12.0 (12 %)	*8.6/6.6 (30 %)*	9.4/9.2 (2 %)
NO$_x$ (ppbv)	*19.6/17.5 (12 %)*	21.2/21.8 (-3 %)	*17.4/23.3 (-25 %)*	14.1/14.2 (-1 %)
CO (ppbv)	*97.8/84.7 (15 %)*	*92.4/88.6 (4 %)*	*70.8/65.9 (7 %)*	83.7/81.4 (3 %)
PM$_{2.5}$ (µg m^{-3})	*6.1/5.5 (11 %)*	*6.7/7.3 (-8 %)*	*5.9/7.8 (-24 %)*	5.5/5.1 (8 %)
PM$_{2.5}$/ΔCO (µg m^{-3} ppbv^{-1})	*0.29/0.62 (-53 %)*	*0.35/0.51 (-31 %)*	0.32/0.37 (-14 %)	0.27/0.33 (-18 %)
Sea-Salt (µg m^{-3})	*47.2/28.4 (66 %)*	*44.1/25.4 (74 %)*	27.0/26.0 (4 %)	*50.6/36.0 (41 %)*
Sea-Salt$_{PM2.5}$ (µg m^{-3})	*6.2/4.0 (55 %)*	*6.2/4.1 (51 %)*	4.9/4.9 (0 %)	*6.8/5.0 (36 %)*
Dust (µg m^{-3})	*0.80/0.91 (-12 %)*	*2.32/3.03 (-23 %)*	*4.47/3.02 (48 %)*	*1.16/1.04 (12 %)*
Dust$_{PM2.5}$ (µg m^{-3})	*0.31/0.34 (-9 %)*	*0.79/1.00 (-21 %)*	*1.58/1.18 (34 %)*	*0.44/0.36 (22 %)*
Sea-Salt/ΔCO (µg m^{-3} ppbv^{-1})	*2.10/2.74 (-23 %)*	*2.54/1.70 (49 %)*	1.50/1.58 (-5 %)	*2.44/1.66 (47 %)*
Sulfate/ΔCO (µg m^{-3} ppbv^{-1})	*0.029/0.055 (-47 %)*	*0.041/0.052 (-21 %)*	0.039/0.046 (-15 %)	0.024/0.027 (-11 %)
Dust/ΔCO (µg m^{-3} ppbv^{-1})	*0.038/0.082 (-54 %)*	*0.129/0.186 (-31 %)*	*0.235/0.152 (55 %)*	0.052/0.047 (11 %)
BC/ΔCO (µg m^{-3} ppbv^{-1})	*0.0031/0.0056 (-45 %)*	*0.0042/0.0057 (-26 %)*	0.0041/0.0049 (-16 %)	0.0032/0.0033 (-3 %)
OC/ΔCO (µg m^{-3} ppbv^{-1})	*0.0093/0.0238 (-61 %)*	*0.0164/0.0276 (-41 %)*	0.0225/0.0287 (-22 %)	*0.0127/0.0153 (-17 %)*
Sea-Salt$_{PM2.5}$/ΔCO (µg m^{-3} ppbv^{-1})	*0.263/0.403 (-35 %)*	*0.352/0.262 (34 %)*	0.284/0.298 (-5 %)	*0.331/0.255 (30 %)*
Dust$_{PM2.5}$/ΔCO (µg m^{-3} ppbv^{-1})	*0.015/0.033 (-55 %)*	*0.042/0.062 (-32 %)*	*0.087/0.053 (64 %)*	0.018/0.017 (6 %)
Wind$_{SF}$ (m s^{-1})	*8.5/7.1 (20 %)*	*8.4/5.9 (42 %)*	4.4/4.7 (-6 %)	*7.7/6.6 (17 %)*
APT$_{6h}$ (mm)	*0.1/0.0 (NaN)*	0.0/0.0 (NaN)	0.0/0.0 (NaN)	0.0/0.0 (NaN)
APT (mm)	*24.7/0.0 (NaN)*	*22.6/0.2 (11200 %)*	*24.1/0.0 (NaN)*	*25.0/0.2 (12400 %)*

	All
V$_f$ /ΔCO × 10^4 (µm^3 µm^{-2} ppbv^{-1})	3.42/7.55 (-55 %)
R$_{eff-f}$ (µm)	0.158/0.147 (7 %)
R$_f$ (µm)	0.176/0.171 (3 %)
σ$_f$	0.471/0.470 (0 %)
V$_c$ /ΔCO × 10^4 (µm^3 µm^{-2} ppbv^{-1})	2.04/2.12 (-4 %)
R$_{eff-c}$ (µm)	1.956/2.085 (-6 %)
R$_c$ (µm)	2.503/2.562 (-2 %)
σ$_c$	*0.684/0.647 (6 %)*

497

498 $^{*}\% \, difference = \frac{X_{High-rain} - X_{Low-rain}}{X_{Low-rain}} \times 100$

499
500   With the normalization technique, $PM_{2.5}/\Delta CO$ exhibits lower values in the high APT
501 category for each season as compared to low APT conditions (Fig. 6), with differences between
502 medians being statistically significant in DJF and MAM based on p-value < 0.05 with a Wilcoxon
503 rank-sum test (Table 2). The DJF season exhibits the greatest reduction of this ratio (by 53%) in
504 high APT conditions (0.29 µg m^{-3} ppbv^{-1} versus 0.62 µg m^{-3} ppbv^{-1} based on median values; Table
505 2). Therefore, these results suggest that it is plausible that wet scavenging has a marked impact on
506 surface $PM_{2.5}$ at a remote ocean site in the WNAO. This also helps support the speculation
507 proposed by Aldhaif et al. (2021) that wet scavenging can reconcile why, in particular for DJF, the
508 high density of trajectories coming from North America correlates with a reduction in fine
509 particulate pollution arriving at Bermuda as compared to other seasons. It is noteworthy that the
510 highest median value of $PM_{2.5}/\Delta CO$ was for the low APT category of DJF providing support for
511 how that season has both greater influence of aerosol transport from North America (when the
512 precipitation scavenging potential is reduced during low APT periods) and the greatest sensitivity
513 to the effects of precipitation over the WNAO owing to the widest range in this ratio's value
514 between high and low APT categories.
515
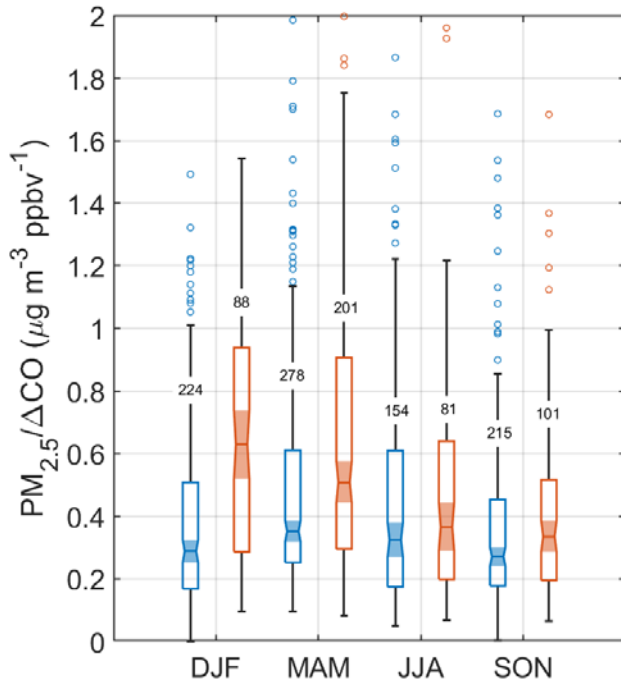
516
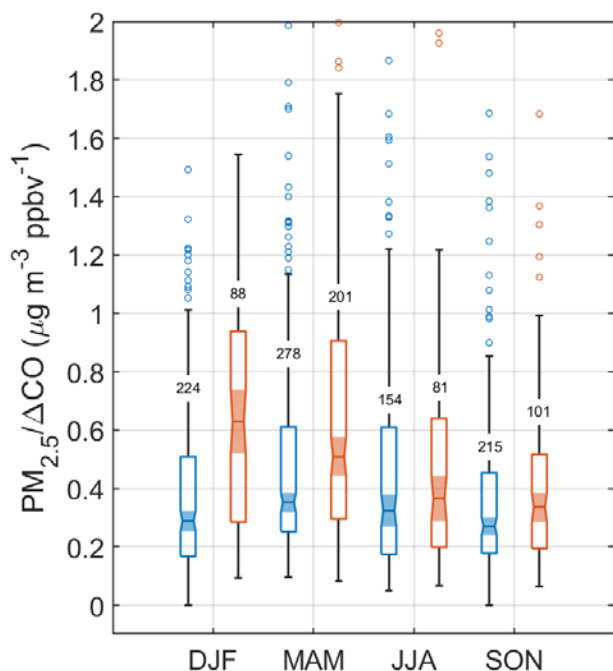
517

Figure 6. Box notch plot for each season comparing the $PM_{2.5}/\Delta CO$ ratio for Cluster 1
trajectories for high-APT (blue) and low-APT (orange) conditions. APT thresholds are based
on 25th (< 0.9 mm) and 75th (> 13.5 mm) percentiles of APT for all trajectories reaching
Bermuda between 1 January 2015 and 31 December 2019. The number of samples in each
group is placed on whiskers.

     Figure 7 additionally shows the seasonal sensitivity of $PM_{2.5}/\Delta CO$ to APT based on four
bins of APT (bin ranges shown in Table S3) chosen in such a way to provide similar numbers of
data points per bin for each particular season. We note that the general trends are preserved using
similar bin ranges in each of the seasons. DJF and MAM show the greatest reductions from the
first to last bin as expected based on Table 2, but these also were the only two seasons showing
reductions between each successive bin. In contrast, SON and JJA exhibited more variable
behavior with $PM_{2.5}/\Delta CO$ actually increasing between a pair of bins in each season. A number of
reasons can potentially explain the less pronounced reduction in $PM_{2.5}/\Delta CO$ for SON and JJA: (i)
lower values to begin with in the lowest APT bins (and thus lower potential for scavenging to
occur); (ii) potential humidity effects associated with air masses at higher APT values promoting
secondary aerosol formation (Huang et al., 2014; Quan et al., 2015; Ding et al., 2021); (iii) more
influence from natural emissions in the form of dust (especially JJA) and sea salt (especially SON)
(Aldhaif et al., 2021). Another noteworthy result is that the season with the clearest scavenging
signature (DJF) shows the most sensitivity (i.e., steepest downward slope) between the first two
APT bins (0.9 mm versus 4.3 mm) as there was a 26% reduction in $PM_{2.5}/\Delta CO$ (0.584 μg m^{-3}
ppbv^{-1} to 0.435 μg m^{-3} ppbv^{-1}), resulting in a slope (units of μg m^{-3} ppbv^{-1} mm^{-1}) of -0.044 in
contrast to slopes of -0.007 and -0.006 for the subsequent two pairs of bins in DJF. Tunved et al.

518
519
520
521
522
523
524
525
526
527
528
529
530
531
532
533
534
535
536
537
538
539

540 (2013) also reported a similar exponential trend between particle mass and accumulated
541 precipitation where an initial rapid decrease in particle mass was followed by a decreased removal
542 rate of aerosol due to precipitation.
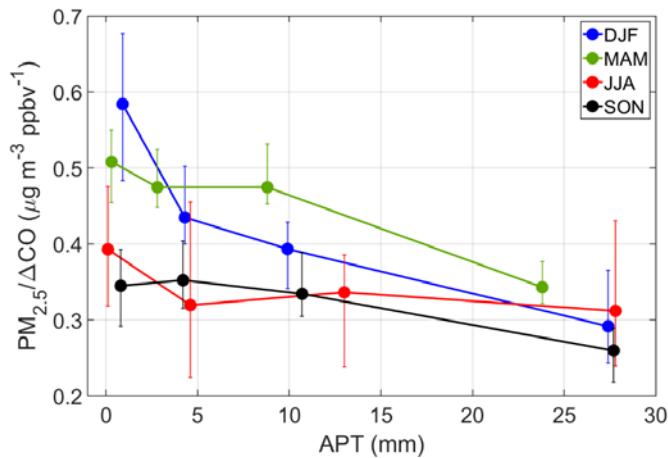
543
544 **Figure 7. Seasonal sensitivity of PM$_{2.5}$/ΔCO to APT for Cluster 1 trajectories, divided based**
545 **on four APT bins that have a similar number of data points per season. Markers denote**
546 **median values and error bars represent the 95% confidence interval for medians based on a**
547 **bootstrapping method (n = 100,000). Number of points per marker: DJF = 192 – 194; MAM**
548 **= 247 – 251; JJA = 107 – 110; SON = 183 – 191.**
549
550   We next address some additional details motivated by values shown in Table 2. We
551 examine three aerosol constituents linked to anthropogenic outflow from North America, including
552 sulfate, black carbon (BC), and organic carbon (OC) from MERRA-2 reanalysis. We recognize
553 that sulfate and OC have non-anthropogenic precursor vapors such as ocean-emitted dimethyl
554 sulfide and biogenic volatile organic compounds, respectively. Being the most abundant of the
555 three, sulfate exhibits the same characteristics as PM$_{2.5}$ when normalized by ΔCO with the sharpest
556 reduction at high APT conditions in DJF, followed by MAM, and then finally by JJA and SON
557 albeit with p-values > 0.05 for the latter two seasons as compared to low APT conditions. BC/ΔCO
558 ratios show the same relative characteristics between APT categories as sulfate/ΔCO for each
559 season, and mostly the same for OC/ΔCO except that the reduction in the median value in high
560 APT conditions for SON was significant (p-value < 0.05). Regardless of season, but most
561 pronounced in DJF, was the consistent result that OC/ΔCO exhibited the highest relative reduction
562 at high APT conditions (versus low APT) compared to BC and sulfate. Further work with more
563 expansive observational data is needed to better understand how different species respond to wet
564 scavenging.
565   Normalization by ΔCO was important for assessing transport efficiency of anthropogenic
566 pollution, but we also considered dust and sea salt without ΔCO normalization as they are
567 predominantly emitted by natural sources. Although outside the scope of this study, we caution
568 that MERRA-2 concentrations of sea salt in the PM$_{2.5}$ fraction may exceed those of total PM$_{2.5}$ as
569 measured at Ft. Prospect (Table 2) owing to the inherent differences in the two respective datasets

570 including the larger spatial scale covered by MERRA-2 as compared to the point measurements at
571 Ft. Prospect. Previous analysis of precipitation scavenging ratios over Bermuda showed that larger
572 aerosol types (e.g., sea salt) are removed more efficiently than smaller aerosol types (e.g., sulfate,
573 nitrate) (Galloway et al., 1993). Total sea salt and sea salt in the $PM_{2.5}$ fraction exhibited higher
574 median concentrations for the high APT category (p-value < 0.05) for all seasons except JJA,
575 which had more comparable values. This can be explained by how ~~the~~days experiencing high APT
576 ~~days~~ exhibited significantly higher surface wind speeds around Bermuda for all seasons except
577 JJA, for which wind speeds in general were depressed. Therefore, the reduction of the $PM_{2.5}/\Delta CO$
578 ratio in high APT conditions may actually be an underestimate of wet scavenging of North
579 American pollution outflow since local sea salt is higher windier days marked by high APT.
580   To put this last assertion on firmer ground, we examined local rain values as they could be
581 influential in terms of scavenging the locally generated sea salt. The median values of local rain
582 on high APT days for each season based on APT for the most recent 6 hours of trajectories arriving
583 at Bermuda (APT_{6h}) were 0.0 – 0.1 mm, while median values of APT_{6h} on low APT days were 0
584 mm in each season. The only significant difference in median APT_{6h} values was in DJF when it
585 was 0.1 mm on high APT days in contrast to 0.0 mm on low APT days. Therefore, for DJF the
586 slightly enhanced APT_{6h} can possibly offset the greater sea salt emissions in terms of impacting
587 $PM_{2.5}$ levels over Bermuda. Results for the other major natural aerosol type (dust) reveal much
588 lower overall concentrations as compared to sea salt for both bulk sizes and the $PM_{2.5}$ fraction.
589 There was no consistent trend across the four seasons in terms of dust levels being higher for either
590 the low or high APT category, which is not unexpected as dust is not a major aerosol type expected
591 from North American outflow (Yu et al., 2020; Corral et al., 2021).

3.3.1 Volume Size Distributions

594   We next examine AERONET volume size distribution (VSD) relationships with APT. We
595 normalize the volume concentration data by corresponding ΔCO in the same way as was done for
596 $PM_{2.5}$, with the same condition of using data only when $\Delta CO > 3.2$ ppbv. A few cautionary details
597 are first noted about these data in comparison to APT: (i) there are limited VSD data in the
598 AERONET dataset, which is why we use all seasons of data together for Fig. 8 and Table 2; (ii)
599 AERONET data are representative of ambient conditions and changes in relative humidity can
600 influence VSD profiles; and (iii) AERONET data are column-based and not necessarily
601 representative of only the surface layer where the trajectories end in our analysis of HYSPLIT
602 data. Related to the last point, past work noted that column optical properties over Bermuda can
603 be weakly correlated with such measurements at the surface (Aryal et al., 2014) due largely to
604 aerosol layers aloft (Ennis and Sievering, 1990). At the same time, studies have shown that there
605 can be enhanced number and volume concentrations in the marine boundary layer versus the free
606 troposphere over Bermuda (Horvath et al., 1990; Kim et al., 1990).
607   The median VSDs for both APT categories exhibit a bimodal profile with a more dominant
608 coarse mode, consistent with what is already known for Bermuda based on AERONET data
609 (Aldhaif et al., 2021). The unique aspect of this work is that in high APT conditions, there is a
610 reduction in median volume concentration in the smaller mode between radii of 0.05 and ~1 μm,
611 with a slight enhancement on the leading shoulder of the larger mode between radii of 1.71 and
612 2.94 μm (Fig. 8). The greatest relative reductions in the fine mode, which is more indicative of
613 transported continental pollution, occurred between midpoint radii of 0.15 and 0.33 μm with
614 relative reductions in those four bins (i.e., midpoint radii = 0.15, 0.19, 0.26, and 0.33 μm) ranging

615 from 38% to 52%. The coarse mode peaked at larger radii (3.86 μm) in low APT conditions relative
616 to high APT conditions (2.94 μm).
617   Table 2 reports VSD parameter values for the APT categories separated by fine and coarse
618 modes. Although only significantly different based on 90% confidence (p-value = 0.09), the fine
619 mode volume concentration normalized by ΔCO in the high APT category was less than half (45%)
620 the value in the low APT category. There were insignificant differences between effective radii
621 and volume median radii, in addition to the geometric standard deviation for the fine mode between
622 APT categories. For the coarse mode, only the geometric standard deviation exhibited a significant
623 difference by being higher in the high APT category (0.684 versus 0.647), although we presume
624 that has less to do with actual scavenging effects and more to do with different times of the year
625 where the relative abundance of different coarse particle type changes.
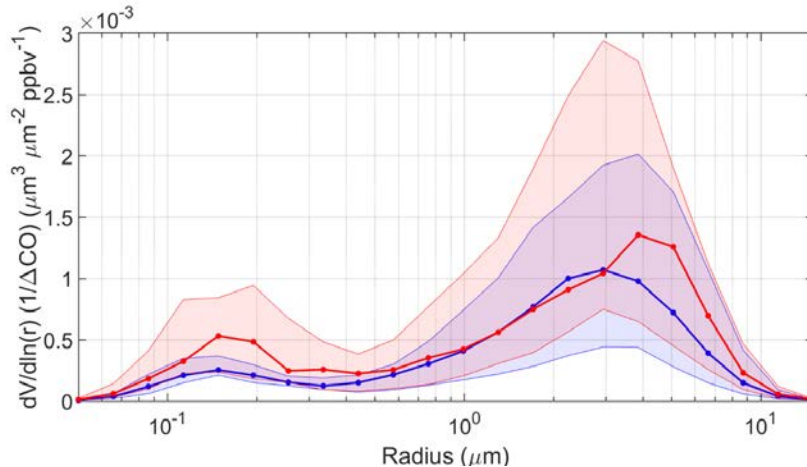
626
627 **Figure 8. Volume size distributions (VSD) normalized by ΔCO for high APT (> 13 mm; blue,**
628 **n = 16) and low APT (< 0.9 mm; red, n = 19) groups for Cluster 1 trajectories. Thick curves**
629 **correspond to medians and shaded areas extend to the 25th and 75th percentiles. VSDs are**
630 **based on AERONET data between 1 January 2015 and 31 December 2019.**
631
632   The AERONET results support the idea that scavenging on high APT days efficiently
633 removes fine particulate matter but that there can still be appreciable levels of locally generated
634 sea salt due to higher local surface winds on high APT days. Related to the columnar nature of
635 AERONET data, it is important to note that others have reported large-scale subsidence of
636 pollution from the mid and upper troposphere, especially in spring, based on enhanced ozone
637 mixing ratios at the surface of Bermuda (Oltmans and Levy, 1992; Cooper et al., 1998; Milne et
638 al., 2000; Li et al., 2002). Moreover, this phenomenon is synoptically favorable with the transport
639 of North American polluted air behind cold fronts especially in spring (Moody et al., 1995) and
640 often linked to the lifting of polluted air out of the boundary layer by convection over the
641 continental U.S. (Prados et al., 1999). It is unclear based on the current dataset how effective these
642 events were in impacting either the surface layer or columnar-based aerosol measurements at
643 Bermuda.
644

3.4 GEOS-Chem Model Results

We conduct four GEOS-Chem simulations of the ^{210}Pb submicron aerosol tracer including a) one standard simulation; b) same as the standard simulation but with the ^{222}Rn tracer emissions from the North American continent (25-60°N, 130-70°W) removed; c) same as the standard simulation but without ^{210}Pb scavenging due to large-scale precipitation; and d) same as the standard simulation but without ^{210}Pb scavenging by convective precipitation. The difference between a) and b) quantifies the North American contribution to atmospheric ^{210}Pb concentrations. The difference between a) and c) reflects the role of large-scale precipitation scavenging, while the difference between a) and d) reflects that of convective precipitation scavenging in determining atmospheric ^{210}Pb concentrations. All model simulations are conducted for the period from September 2016 to December 2017 with the first four months for spin-up. Monthly mean outputs for 2017 are used for analysis, which is a representative year within the time frame of the analysis presented in Sections 3.1-3.3. This is confirmed by the seasonal APT box chart constructed in Fig. S6 using only 2017 data, which nearly follows the trend observed when the five-year data are used (Fig. 5).
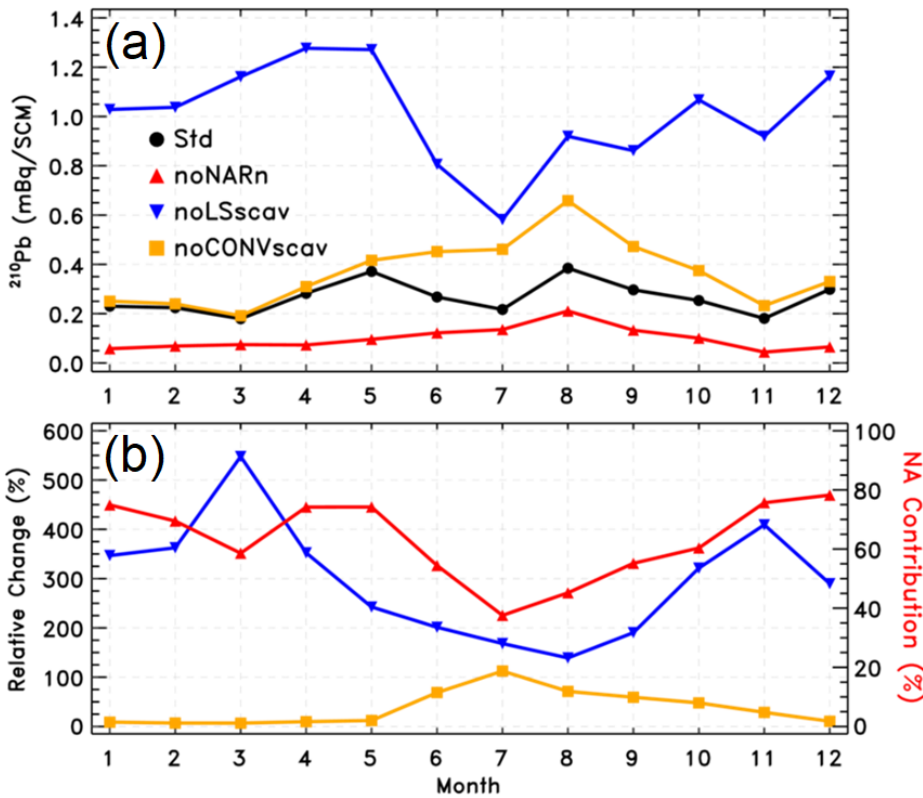
Figure 9. Simulated monthly surface ^{210}Pb tracer concentrations submicron mBq/SCM at Bermuda (32.31° N, 64.75° W) in 2017 as a way to assess effects of precipitation scavenging

663 **on North American outflow. Panel (a): monthly mean surface ^{210}Pb concentrations in**
664 **the standard simulation ("Std") and three sensitivity simulations, i.e., without North**
665 **American ^{222}Rn emissions ("noNARn"), without large-scale precipitation scavenging**
666 **("noLSscav"), and without convective precipitation scavenging ("noCONVscav"). Panel (b):**
667 **percentage changes, i.e., (noLSscav-Std)/Std×100 in blue and (noCONVscav-Std)/Std×100 in**
668 **orange, and the North American contribution in red, i.e., (Std–noNARn)/Std×100.**
669
670   Figure 9a shows monthly mean surface ^{210}Pb concentrations at Bermuda for 2017 in
671 the standard simulation and three sensitivity simulations. Figure 9b plots the relative changes in
672 simulated ^{210}Pb concentrations due to the effects of large-scale or convective precipitation
673 scavenging. Also included in Fig. 9b is the North American contribution. The standard model
674 simulates a seasonality in ^{210}Pb concentrations with two distinct peaks in May and August (upper
675 panel). The May peak is a result of increased transport from North America in combination with
676 reduced scavenging. In contrast, the August peak results from long-range transport from other
677 continents (e.g., North Africa, Europe) along the southern edge of the Bermuda High. The lows in
678 March and November are attributed to strong large-scale precipitation scavenging, and the low in
679 July is associated with enhanced convective precipitation scavenging. The sensitivity simulations
680 clearly show that the role of large-scale precipitation scavenging in affecting surface ^{210}Pb
681 concentrations at Bermuda is much larger in winter/spring than in summer, with a maximum in
682 March (lower panel), while convective scavenging also plays an important role in summer. The
683 relative contribution of North American ^{222}Rn emissions is largest in winter (~75-80%), suggesting
684 air masses reaching Bermuda often experience large-scale precipitation scavenging while
685 traveling from the North American continent during winter. ~~These~~While the model may have
686 limitations and inherent uncertainties, its results are ~~thus~~at least consistent with ~~previous~~ results
687 shown already ~~and put~~, putting our conclusions on firmer ground.
688
689 **3.5 Airborne Case Study**
690   The DJF season has been shown in this study to ~~unite~~exhibit the greatest potential for wet
691 scavenging and the highest density of trajectories from North America reaching Bermuda. To
692 probe deeper now, we take advantage of data from ACTIVATE RF6 on 22 February 2020, which
693 characterized the intermediate region between North America and Bermuda. Weather in the
694 ACTIVATE domain on this day was characterized by a transition from post-cold front conditions
695 to high pressure. A cold front passed over Bermuda the previous day at approximately 18:00 UTC
696 on 21 February, and by the flight period of RF06 was approximately 600 km southeast of the
697 island. Meanwhile, a broad but weakening area of surface high pressure continued eastward into
698 the southeast U. S. Winds in the boundary layer were southwesterly at around 5 m s^{-1} near the base
699 of operations (NASA Langley Research Center; Hampton, Virginia), which were associated with
700 a weak trough on the northeast side of the high pressure system. These winds shifted to north-
701 northwest near the coast at 2.5 m s^{-1} and north-northeast at 7.4 m s^{-1} near the far end of the flight
702 track; Bermuda reported north-northeast winds around 9 m s^{-1} during this period. Aloft, 500 hPa
703 flow was from the west-northwest. NASA Langley reported few to no clouds during the flight
704 period, while Bermuda reported broken clouds with multiple layers (with bases around 900 m and
705 1800 m) and rain showers at or near the airport. This is consistent with satellite imagery (Fig. 10a),
706 which shows an area of scattered to broken cumulus and stratocumulus extending from the cold
707 front near Bermuda to the edge of the Gulf Stream off the U.S. East Coast. Satellite-retrieved cloud
708 bases were at 1–2 km, with cloud tops ranging from 1.5–3.5 km; from the HU-25 Falcon flight

709 legs, cloud bases encountered along the flight track were 750–1100 m and cloud tops were 1200–
710 1800 m.
711

712

713
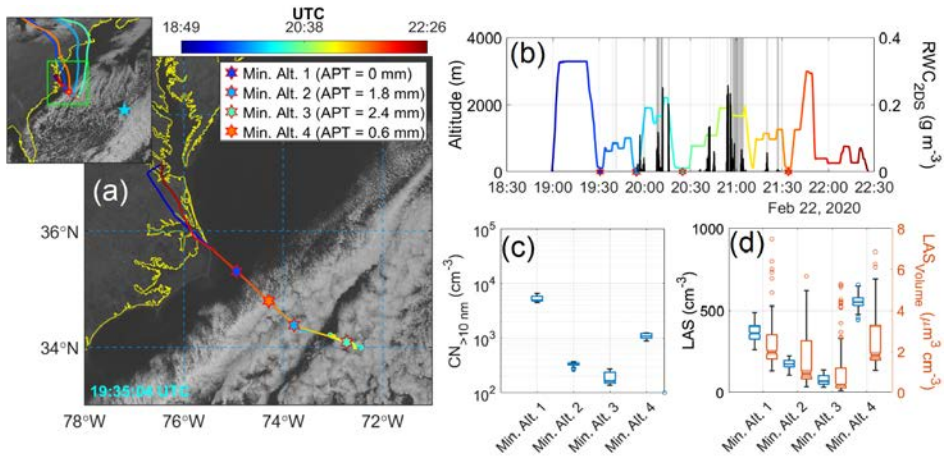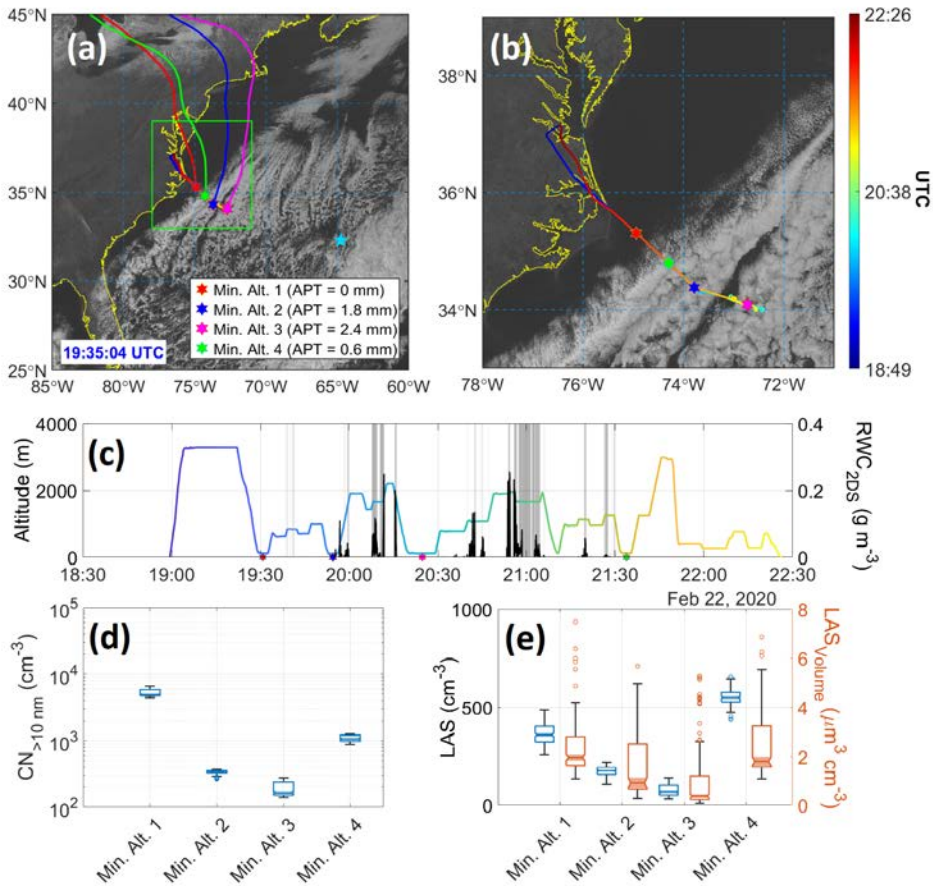
Figure 10. Summary of ACTIVATE's Research Flight 6 on 22 February 2020. (a) HU-25 **Falcon flight track overlaid on GOES-16 imagery** ~~with the smaller figure to the top left being~~ ~~a zoomed-out version~~ **of the WNAO (Bermuda denoted by blue star)** ~~and the larger figure~~ ~~zooming in on the area of the flight path.~~ also showing 96 hour back-trajectories calculated for each respective Min Alt. leg. **The midpoint of the four Min. Alt. legs are marked** ~~along~~ ~~with~~including **values for the accumulated precipitation along the trajectory (APT) for the** **recent history of the sampled air masses when they were over the ocean (time over land** **excluded from APT calculation).** ~~(b)~~(b) Zoomed in version of panel (a) focused on the flight path. (c) **Time series of Falcon altitude colored by flight UTC time (color bar in panel** ~~a~~b) **and rain water content (RWC) from the 2DS probe. Gray shaded bars signify when FCDP** **liquid water content exceeded 0.05 g m⁻³, indicative of cloud legs. The same four colored stars** **from (a) are shown on the x-axis to indicate where they occurred. (**~~c~~d-e**) Box notch plots of** **the leg-mean Min. Alt. values of CPC particle** ~~(> 10 nm)~~ **concentration**~~,~~ (> 0.01 μm), **and the** **number and volume concentrations of the LAS (> 0.09 μm).**

728

729   Figure 10a shows the general flight path, which involved flying to a point southeast of the
730   operations base (Hampton, Virginia) and then re-tracing the path back to land. Four HYSPLIT
731   back-trajectories are shown (Fig. 10a) corresponding to midpoints of each Min. Alt. leg when the
732   aircraft was at its lowest altitude (~500 ft). APT calculations were conducted for segments of those
733   four trajectories that were over the ocean. As a successful validation of the technique, no to focus
734   on wet removal clouds over the WNAO. Negligible rain accumulated up to the point of the Min.
735   Alt. 1 leg, as there were cloud-free conditions between land and that offshore point. In contrast,
736   the next three Min. Alt. legs show higher APT values ranging from 0.6 to 2.4 mm, consistent with
737   the GOES-16 imagery showing cloud fraction increasing just to the southeast of the Min. Alt. 1
738   leg. Expectedly, APT values progressively increased with offshore distance as a result of air
739   masses being exposed to clouds for longer periods. Figure S7 shows 27 trajectories obtained for
740   each Min. Alt. leg based on ensemble trajectory analysis which is a technique available in
741   HYSPLIT to evaluate uncertainties in trajectory calculations by offsetting the meteorological data
742   by a fixed grid factor. Average APT values based on ensemble analysis (Fig. S7) were 0.29, 1.18,
743   2.27, and 0.73 mm corresponding to Min. Alt. 1, 2, 3, and 4 legs, respectively, which follow the
744   trend observed in Fig. 10.
745   Shortly after the Min. Alt. 1 leg, the Falcon conducted two consecutive pairs of BCB and
746   ACB legs (i.e., below cloud base followed by above cloud base), followed by a slant descent to
747   the Min. Alt. 2 leg, where RWC values were enhanced (up to 0.02 g m^{-3} at 19:55:22 UTC) owing
748   to precipitation from overlying clouds. Very shortly thereafter, RWC reached as high as 0.11 g m^{-3}
749   (19:56:50 UTC) in the slant ascent profile passing through clouds. The APT value in Min. Alt. 2
750   leg was 1.8 mm. A significant reduction was observed in the aerosol number and volume
751   concentrations for the Min. Alt. 2 leg as compared to the Min. Alt. 1 leg (Figs. 10c-d).10d-e).
752   Table S4 reports the statistics for aerosol parameters measured in Min. Alt. legs (Fig. 10). CPC (>
753   10 nm) concentrations dropped by 93% from a leg-median value of 4938 cm^{-3} during Min. Alt. 1
754   to 345 cm^{-3} during Min. Alt. 2, whereas the LAS number and volume (> 100 nm) concentrations
755   dropped from 360 cm^{-3} to 174 cm^{-3} and from 2.0 µm^3 cm^{-3} to 0.9 µm^3 cm^{-3}, respectively. Size
756   distribution data in those two legs show a significant reduction in particle concentration across the
757   full diameter range as measured by the SMPS and LAS (Fig. 11). A notable feature from the SMPS
758   was a pronounced peak between 3.5 – 14.1 nm suggestive of nucleation, that was absent in
759   subsequent Min. Alt. legs, presumably owing to some combination of coagulation and scavenging.

760
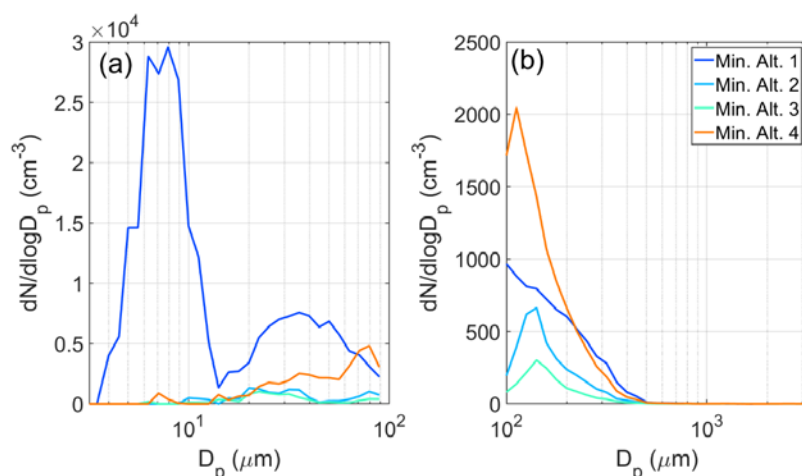
Figure 11. Aerosol size distribution comparison (a = SMPS, b = LAS) between the four HU-25 Falcon Min. Alt. legs during ACTIVATE Research Flight 6, as shown in Fig. 10.

763

764   The aircraft continued southeast after the Min. Alt. 2 leg and passed through more patches
765 of precipitation, leading to the highest APT value of 2.4 mm in the Min. Alt. 3 leg, where leg-
766 median values were as follows: CPC = 165 cm^{-3}, LAS number = 66 cm^{-3}, LAS volume = 0.4 µm^3
767 cm^{-3}. While the SMPS distributions in the Min. Alt. 2 and 3 legs were very similar, the LAS size
768 distribution in the Min. Alt. 3 leg is shifted towards lower concentrations, especially below 400
769 nm. On the path back towards Virginia, the Falcon conducted one final Min. Alt. 4 leg right before
770 the boundary between cloudy and clear air, with the APT value being 0.6 mm. Between the Min.
771 Alt. 3 and 4 legs, again, significant RWC values were observed reaching as high as 0.26 g m^{-3} at
772 20:54:20 UTC. Aerosol concentration measurements increased relative to the Min. Alt. 2 and 3
773 legs (leg-median values): CPC = 1076 cm^{-3}, LAS number = 545 cm^{-3}, LAS volume = 1.8 µm^3 cm^{-}
774 ^{3}. It is difficult to compare results from the Min. Alt. 1 and 4 legs as ~2 hours had passed and there
775 were different conditions impacting the two respective sampled air masses. The size distributions
776 varied considerably for the Min. Alt. 4 leg as compared to the other three legs with increased
777 concentrations between 20-200 nm, presumably as a result of continued pollution outflow and
778 more photochemistry and aerosol growth processing as compared to earlier in the day.
779   To conclude, it is plausible based on the case flight data that the emerging presence of
780 clouds and precipitation led to the substantial reduction of aerosol particles with distance offshore
781 via wet scavenging processes. Further research is warranted with more extensive data to move
782 closer to showing causal relationships between precipitation and aerosol particles. For instance, a
783 few points of caution from RF6 are worth mentioning. First, the coastal trajectories in Fig. 10
784 corresponding to the different Min Alt. legs originated from varying places extending from the
785 Virginia coast up north towards Cape Cod, Massachusetts. Secondly, cloud dynamics and
786 boundary layer structure can vary offshore. Related to the latter, PBLH data obtained from
787 MERRA-2 along the flight track revealed that there were deeper boundary layers farther offshore,
788 but not sufficiently deeper to fully explain the reductions in aerosol concentration: PBLH

789 corresponding to Min. Alt. 1/2/3/4 = 1156/1728/1740/1530 m. Lastly, aerosol concentrations
790 linked to continental outflow naturally decrease anyways offshore, including in cloud-free
791 conditions, owing to dilution during transport.
792
793 **4. Conclusion**

794   This study examines the sensitivity of surface aerosol characteristics over a remote area of
795 the western North Atlantic Ocean (Bermuda) to precipitation along trajectories coming from North
796 America. Based on trajectory clustering with HYSPLIT data, two characteristic transport corridors
797 to Bermuda's surface layer (100 m AGL) were identified, with the focus being the one coming
798 from North America (Cluster 1). Seasonal analysis of HYSPLIT and Bermuda surface data showed
799 that JJA is distinct in terms of having transport from the southeast with the other seasons, especially
800 DJF, having more North American influence with higher concentrations of CO. Comparing Cluster
801 1 trajectories data between high (>13.5 mm) and low (<0.9 mm) accumulated precipitation along
802 trajectories (APT~~,~~), there was a clear signature of wet scavenging effects by precipitation with
803 more than a two-fold reduction in $PM_{2.5}/\Delta CO$ in DJF (0.29 µg m^{-3} ppbv^{-1} versus 0.62 µg m^{-3} ppbv^{-1}
804), with the reduction being less severe for other seasons. The greatest sensitivity of $PM_{2.5}/\Delta CO$ to
805 APT was at the lowest values (up to ~5 mm; slope of -0.044 µg m^{-3} ppbv^{-1} mm^{-1}), above which
806 the descending slope of $PM_{2.5}/\Delta CO$ versus APT was less steep.
807   Speciated data indicate that anthropogenic species such as sulfate, black carbon, and
808 organic carbon are reduced as a function of APT (much like $PM_{2.5}$). However, sea salt was not
809 necessarily reduced and at times could even be higher at Bermuda with high APT conditions,
810 which is attributed to higher local wind speeds ~~and emissions at the surface on days simultaneous~~
811 ~~with high APT trajectories.~~. Analysis of AERONET volume size distribution data at Bermuda
812 confirms the substantial reduction of fine mode volume concentrations in contrast to ~~less~~a smaller
813 change in the coarse mode on high APT days. GEOS-Chem simulations of the radionuclide aerosol
814 tracer ^{210}Pb confirm that North American influence at the surface of Bermuda is highest in DJF,
815 with those air masses significantly impacted by large-scale (i.e., stratiform and anvil) precipitation
816 scavenging; furthermore, convective scavenging is shown to play an important role in summer
817 months. A research flight from ACTIVATE on 22 February 2020 demonstrates a significant
818 gradient in aerosol number and volume concentrations offshore of North America as soon as
819 trajectories start passing across clouds, consistent with increasing APT away from the coast
820 leading to increased aerosol particle removal.
821   Our results have implications for other remote marine regions impacted by transport of
822 continental emissions. These results also highlight the important role of precipitation in modifying
823 aerosol levels, including potentially their vertical distribution (e.g., Luan and Jaeglé, 2013), along
824 continental outflow trajectories. We show that cloud and precipitation processes along trajectories
825 have significant impacts on resultant aerosol characteristics~~, suggesting that wet~~. Therefore, it is
826 important to strongly constrain we scavenging processes in models ~~require stronger constraints~~
827 ~~than other~~ to improve aerosol ~~microphysical/chemical processes to improve the~~ forecasting ~~of~~
828 ~~aerosol properties in marine atmospheres.~~over the WNAO
829
830
831

832 *Data Availability.*

833 Fort Prospect Station Aerosol/Gas Measurements:
834 https://doi.org/10.6084/m9.figshare.13651454.v2

835 AERONET: https://aeronet.gsfc.nasa.gov/

836 HYSPLIT: https://www.ready.noaa.gov/HYSPLIT.php

837 MERRA-2: https://disc.gsfc.nasa.gov/

838 GEOS-Chem Model: http://wiki.seas.harvard.edu/geos-chem/index.php/GEOS-Chem_v11-01

839 Section 3.5 ACTIVATE Airborne Data:
840 https://doi.org/10.5067/SUBORBITAL/ACTIVATE/DATA001

841 Section 3.5 airport weather data: http://mesonet.agron.iastate.edu/ASOS/

842 Section 3.5 ocean surface analysis charts and GFS 500 hPa analysis:
843 https://www.ncei.noaa.gov/data/ncep-charts/access/

844 Section 3.5 North America Analysis/Satellite composite:
845 https://www.wpc.ncep.noaa.gov/archives/web_pages/sfc/sfc_archive_maps.php

846 Section 3.5 Satellite imagery/products: https://satcorps.larc.nasa.gov/cgi-
847 bin/site/showdoc?docid=4&cmd=field-experiment-homepage&exp=ACTIVATE

848 *Author contributions.* HD and MA conducted the analysis. AS and HD prepared the manuscript.
849 HL and BZ performed GEOS-Chem model radionuclide simulations and output analysis. All
850 authors contributed by providing input and/or participating in airborne data collection.

851 *Competing interests.* The authors declare that they have no conflict of interest.

852 *Acknowledgments.* The work was funded by NASA grant 80NSSC19K0442 in support of
853 ACTIVATE, a NASA Earth Venture Suborbital-3 (EVS-3) investigation funded by NASA's Earth
854 Science Division and managed through the Earth System Science Pathfinder Program Office. HL
855 and BZ acknowledge support from NASA grant 80NSSC19K0389. The AERONET station in
856 Bermuda is maintained on behalf of NASA by the Bermuda Institute of Ocean Sciences at the
857 Tudor Hill Marine Atmospheric Observatory, which is currently supported by NSF award
858 1829686, and by previous such awards during the time period in this study. Gas chemistry and PM
859 data at Fort Prospect are from the Bermuda Air Quality Program, operated by BIOS with funding
860 from the Department of Environment and Natural Resources, Government of Bermuda. The
861 authors acknowledge the NOAA Air Resources Laboratory (ARL) for the provision of the
862 HYSPLIT transport and dispersion model and READY website (http://ready.arl.noaa.gov) used in
863 this work. The Pacific Northwest National Laboratory (PNNL) is operated for DOE by the Battelle
864 Memorial Institute under contract DE-AC05-76RLO1830. The NASA Center for Climate
865 Simulation (NCCS) provided supercomputing resources. The GEOS-Chem model is managed by
866 the Atmospheric Chemistry Modeling Group at Harvard University with support from NASA

867 ACMAP and MAP programs. GEOS-Chem input files were obtained from the GEOS-Chem Data
868 Portal enabled by Compute Canada.

869

870 **References**

871 Aldhaif, A. M., Lopez, D. H., Dadashazar, H., Painemal, D., Peters, A. J., and Sorooshian, A.:
872 An Aerosol Climatology and Implications for Clouds at a Remote Marine Site: Case Study Over
873 Bermuda, Journal of Geophysical Research: Atmospheres, 126, e2020JD034038,
874 https://doi.org/10.1029/2020JD034038, 2021.

875 Altieri, K. E., Hastings, M. G., Gobel, A. R., Peters, A. J., and Sigman, D. M.: Isotopic
876 composition of rainwater nitrate at Bermuda: The influence of air mass source and chemistry in
877 the marine boundary layer, J Geophys Res-Atmos, 118, 11304-1131611, 304–11, 316,
878 https://doi.org/10.1002/jgrd.50829, 2013.

879 Anderson, J. R., Buseck, P. R., Patterson, T. L., and Arimoto, R.: Characterization of the
880 Bermuda tropospheric aerosol by combined individual-particle and bulk-aerosol analysis, Atmos
881 Environ, 30, 319-338, 1996.https://doi.org/10.1016/1352-2310(95)00170-4, 1996.

882 Arimoto, R., Duce, R. A., Savoie, D. L., and Prospero, J. M.: Trace-Elements in Aerosol-
883 Particles from Bermuda and Barbados - Concentrations, Sources and Relationships to Aerosol
884 Sulfate, J Atmos Chem, 14, 439-457, https://doi.org/10.1007/BF00115250,1992.

885 Arimoto, R., Duce, R. A., Ray, B. J., Ellis, W. G., Cullen, J. D., and Merrill, J. T.: Trace-
886 Elements in the Atmosphere over the North-Atlantic, J Geophys Res-Atmos, 100, 1199-1213,
887 https://doi.org/10.1029/94jd02618, 1995.

888 Arimoto, R., Snow, J. A., Graustein, W. C., Moody, J. L., Ray, B. J., Duce, R. A., Turekian, K.
889 K., and Maring, H. B.: Influences of atmospheric transport pathways on radionuclide activities in
890 aerosol particles from over the North Atlantic, J Geophys Res-Atmos, 104, 21301-21316,
891 1999.https://doi.org/10.1029/1999JD900356, 1999.

892 Arimoto, R.: Eolian Dust and Climate: Relationships to Sources, Tropospheric Chemistry,
893 Transport and Deposition. Earth-Science Reviews, 54(1), 29-42, https://doi.org/10.1016/S0012-
894 8252(01)00040-X, 2001.

895 Aryal, R. P., Voss, K. J., Terman, P. A., Keene, W. C., Moody, J. L., Welton, E. J., and Holben,
896 B. N.: Comparison of surface and column measurements of aerosol scattering properties over the
897 western North Atlantic Ocean at Bermuda, Atmos Chem Phys, 14, 7617-7629,
898 2014.https://doi.org/10.5194/acp-14-7617-2014, 2014.

899 Bey, I., Jacob, D. J., Yantosca, R. M., Logan, J. A., Field, B. D., Fiore, A. M., Li, Q. B., Liu, H.,
900 Mickley, L. J. and Schultz, M. G.: Global modeling of tropospheric chemistry with assimilated
901 meteorology: Model description and evaluation, J. Geophys. Res. Atmos., 106(D19), 23073–
902 23095, https://doi.org/10.1029/2001JD000807, 2001.

903 Brattich, E., Liu, H., Tositti, L., Considine, D. B., and Crawford, J. H.: Processes controlling the
904 seasonal variations in ^{210}Pb and ^{7}Be at the Mt. Cimone WMO-GAW global station, Italy: a

905   model analysis, Atmos. Chem. Phys., 17(2), 1061-1080, https://doi.org/10.5194/acp-17-1061-
906   2017, 2017.

907   Cabello, M., Orza, J.A.G., Galiano, V., Ruiz, G.: Influence of meteorological input data on
908   backtrajectory cluster analysis – a seven-year study for southeastern Spain. Advances in Science
909   and Research 2, 65–70, https://doi.org/10.5194/asr-2-65-2008, 2008.

910   Chen, L. Q., and Duce, R. A.: The Sources of Sulfate, Vanadium and Mineral Matter in Aerosol-
911   Particles over Bermuda, Atmos Environ, 17, 2055-2064, 1983.https://doi.org/10.1016/0004-
912   6981(83)90362-1, 1983.

913   Cooper, O. R., Moody, J. L., Davenport, J. C., Oltmans, S. J., Johnson, B. J., Chen, X., Shepson,
914   P. B., and Merrill, J. T.: Influence of springtime weather systems on vertical ozone distributions
915   over three North American sites, J Geophys Res-Atmos, 103, 22001-22013,
916   1998.https://doi.org/10.1029/98JD01801, 1998.

917   Corral, A. F., Braun, R. A., Cairns, B., Gorooh, V. A., Liu, H., Ma, L., Mardi, A. H., Painemal,
918   D., Stamnes, S., van Diedenhoven, B., Wang, H., Yang, Y., Zhang, B., and Sorooshian, A.: An
919   Overview of Atmospheric Features Over the Western North Atlantic Ocean and North American
920   East Coast – Part 1: Analysis of Aerosols, Gases, and Wet Deposition Chemistry, Journal of
921   Geophysical Research: Atmospheres, 126, e2020JD032592,
922   https://doi.org/10.1029/2020JD032592, 2021.

923   Cutter, G. A.: Metalloids in Wet Deposition on Bermuda - Concentrations, Sources, and Fluxes,
924   J Geophys Res-Atmos, 98, 16777-16786, 1993.https://doi.org/10.1029/93JD01689, 1993.

925   Dadashazar, H., Painemal, D., Alipanah, M., Brunke, M., Chellappan, S., Corral, A. F., Crosbie,
926   E., Kirschler, S., Liu, H., Moore, R., Robinson, C., Scarino, A. J., Shook, M., Sinclair, K.,
927   Thornhill, K. L., Voigt, C., Wang, H., Winstead, E., Zeng, X., Ziemba, L., Zuidema, P., and
928   Sorooshian, A.: Cloud Drop Number Concentrations over the Western North Atlantic Ocean:
929   Seasonal Cycle, Aerosol Interrelationships, and Other Influential Factors, Atmos. Chem. Phys.
930   Discuss., 2021, 1-36, https://doi.org/10.5194/acp-2021-153, 2021.

931   Davis, R. E., Hayden, B. P., Gay, D. A., Phillips, W. L., and Jones, G. V.: The North Atlantic
932   Subtropical Anticyclone, J Climate, 10, 728-744, https://doi.org/10.1175/1520-
933   0442(1997)010<0728:tnasa>2.0.co;2, 1997.

934   Dimitriou, K., Remoundaki, E., Mantas, E., Kassomenos, P.: Spatial distribution of source areas
935   of PM$_{2.5}$ by Concentration Weighted Trajectory (CWT) model applied in PM2.5 concentration
936   and composition data, Atmospheric Environment 116, 138–145,
937   doi:https://doi.org/10.1016/j.atmosenv.2015.06.021, 2015.

938   Ding, J., Dai, Q., Zhang, Y., Xu, J., Huangfu, Y., Feng, Y.: Air humidity affects secondary
939   aerosol formation in different pathways, Science of The Total Environment 759, 143540,
940   doi:https://doi.org/10.1016/j.scitotenv.2020.143540, 2021.

942   Dubovik, O., Holben, B., Eck, T. F., Smirnov, A., Kaufman, Y. J., King, M. D., Tanré, D., and
943   Slutsker, I.: Variability of Absorption and Optical Properties of Key Aerosol Types Observed in

Worldwide Locations, J Atmos Sci, 59, 590-608, https://doi.org/10.1175/1520-0469(2002)059<0590:VOAAOP>2.0.CO;2, 2002.

Eastham, S. D., Weisenstein, D. K. and Barrett, S. R. H.: Development and evaluation of the unified tropospheric-stratospheric chemistry extension (UCX) for the global chemistry-transport model GEOS-Chem, Atmos. Environ., 89, 52–63, doi:https://doi.org/10.1016/j.atmosenv.2014.02.001, 2014.

Engström, A., Magnusson, L.: Estimating trajectory uncertainties due to flow dependent errors in the atmospheric analysis. Atmospheric Chemistry and Physics 9, 8857–8867, https://doi.org/10.5194/acp-9-8857-2009, 2009.

Ennis, G., and Sievering, H.: Vertical Profile of Elemental Concentrations in Aerosol Particles in the Bermuda Area during Gce/Case/Watox, Global Biogeochem Cy, 4, 179-188, 1990.https://doi.org/10.1029/GB004i002p00179, 1990.

Galloway, J. N., Tokos, J. J., Knap, A. H., and Keene, W. C.: Local influences on the composition of precipitation on Bermuda, Tellus B: Chemical and Physical Meteorology, 40, 178-188, https://doi.org/10.3402/tellusb.v40i3.15905, 1988.

Galloway, J. N., Keene, W. C., Artz, R. S., Miller, J. M., Church, T. M., and Knap, A. H.: Processes controlling the concentrations of SO(4)(=), NO(3)(-), NH(4)(+), H(+), HCOO(T) and CH(3)COO(T) in precipitation on Bermuda, Tellus B, 41, 427-443, 1989.

Galloway, J. N., Savoie, D. L., Keene, W. C., and Prospero, J. M.: The Temporal and Spatial Variability of Scavenging Ratios for Nss Sulfate, Nitrate, Methanesulfonate and Sodium in the Atmosphere over the North-Atlantic Ocean, Atmos Environ a-Gen, 27, 235-250, 1993.https://doi.org/10.1016/0960-1686(93)90354-2, 1993.

Garrett, T., Zhao, C., Novelli, P.: Assessing the relative contributions of transport efficiency and scavenging to seasonal variability in Arctic aerosol. Tellus B: Chemical and Physical Meteorology 62, 190–196, doi:https://doi.org/10.1111/j.1600-0889.2010.00453.x, 2010.

Gebhart, K.A., Schichtel, B.A., Barna, M.G.: Directional Biases in Back Trajectories Caused by Model and Input Data. Journal of the Air & Waste Management Association, 55, 1649–1662, https://doi.org/10.1080/10473289.2005.10464758, 2005.

Gelaro, R., McCarty, W., Suarez, M. J., Todling, R., Molod, A., Takacs, L., Randles, C. A., 886 Darmenov, A., Bosilovich, M. G., Reichle, R., Wargan, K., Coy, L., Cullather, R., Draper, C., Akella, S., Buchard, V., Conaty, A., da Silva, A. M., Gu, W., Kim, G. K., Koster, R., Lucchesi, R., Merkova, D., Nielsen, J. E., Partyka, G., Pawson, S., Putman, W., Rienecker, M., Schubert, S. D., Sienkiewicz, M., and Zhao, B.: The Modern-Era Retrospective Analysis for Research and Applications, Version 2 (MERRA-2), J Climate, 30, 5419-5454, https://doi.org/10.1175/Jcli-D-16-0758.1, 891 2017.

Giles, D. M., Sinyuk, A., Sorokin, M. G., Schafer, J. S., Smirnov, A., Slutsker, I., Eck, T. F., Holben, B. N., Lewis, J. R., Campbell, J. R., Welton, E. J., Korkin, S. V., and Lyapustin, A. I.: Advancements in the Aerosol Robotic Network (AERONET) Version 3 database – automated

near-real-time quality control algorithm with improved cloud screening for Sun photometer aerosol optical depth (AOD) measurements, Atmos. Meas. Tech., 12, 169-209, https://doi.org/10.5194/amt-12-169-2019, 2019.

Govender, P. and Sivakumar, V.: Application of k-means and hierarchical clustering techniques for analysis of air pollution: A review (1980–2019), Atmospheric Pollution Research, 11, 40–56, https://doi.org/10.1016/j.apr.2019.09.009, 2020.

Government of Bermuda: 2016 Population and Housing Census Report. Retrieved from https://www.gov.bm/articles/2016-population-and-housing-census-report, 2019.

Hilario, M. R. A., Cruz, M. T., Bañaga, P. A., Betito, G., Braun, R. A., Stahl, C., Cambaliza, M. O., Lorenzo, G. R., MacDonald, A. B., AzadiAghdam, M., Pabroa, P. C., Yee, J. R., Simpas, J. B., and Sorooshian, A.: Characterizing Weekly Cycles of Particulate Matter in a Coastal Megacity: The Importance of a Seasonal, Size-Resolved, and Chemically Speciated Analysis, Journal of Geophysical Research: Atmospheres, 125, e2020JD032614, https://doi.org/10.1029/2020JD032614, 2020.

Hilario, M. R. A., Crosbie, E., Shook, M., Reid, J. S., Cambaliza, M. O. L., Simpas, J. B. B., Ziemba, L., DiGangi, J. P., Diskin, G. S., Nguyen, P., Turk, F. J., Winstead, E., Robinson, C. E., Wang, J., Zhang, J., Wang, Y., Yoon, S., Flynn, J., Alvarez, S. L., Behrangi, A., and Sorooshian, A.: Measurement report: Long-range transport patterns into the tropical northwest Pacific during the CAMP2Ex aircraft campaign: chemical composition, size distributions, and the impact of convection, Atmos. Chem. Phys., 21, 3777-3802, https://doi.org/10.5194/acp-21-3777-2021, 2021.

Holben, B. N., Eck, T. F., Slutsker, I., Tanré, D., Buis, J. P., Setzer, A., Vermote, E., Reagan, J. A., Kaufman, Y. J., Nakajima, T., Lavenu, F., Jankowiak, I., and Smirnov, A.: AERONET—A Federated Instrument Network and Data Archive for Aerosol Characterization, Remote Sens Environ, 66, 1-16, https://doi.org/10.1016/S0034-4257(98)00031-5, 1998.

Horvath, H., Gunter, R. L., and Wilkison, S. W.: Determination of the Coarse Mode of the Atmospheric Aerosol Using Data from a Forward-Scattering Spectrometer Probe, Aerosol Sci Tech, 12, 964-980, https://doi.org/10.1080/02786829008959407, 1990.

Hsu, Y.-K., Holsen, T.M., Hopke, P.K.: Comparison of hybrid receptor models to locate PCB sources in Chicago. Atmospheric Environment 37, 545–562, https://doi.org/10.1016/s1352-2310(02)00886-5, 2003.

Huang, S., Arimoto, R., Rahn, K.A.: Changes in atmospheric lead and other pollution elements at Bermuda. Journal of Geophysical Research 101, 21033–21040, https://doi.org/10.1029/96jd02001, 1996.

Huang, R.-J., Zhang, Y., Bozzetti, C., Ho, K.-F., Cao, J.-J., Han, Y., Daellenbach, K.R., Slowik, J.G., Platt, S.M., Canonaco, F., Zotter, P., Wolf, R., Pieber, S.M., Bruns, E.A., Crippa, M., Ciarelli, G., Piazzalunga, A., Schwikowski, M., Abbaszade, G., Schnelle-Kreis, J., Zimmermann, R., An, Z., Szidat, S., Baltensperger, U., Haddad, I.E., Prévôt, A.S.H.: High secondary aerosol

contribution to particulate pollution during haze events in China, Nature 514, 218–222, https://doi.org/10.1038/nature13774, 2014.

Huang, S. L., Rahn, K. A., Arimoto, R., Graustein, W. C., and Turekian, K. K.: Semiannual cycles of pollution at Bermuda, J Geophys Res-Atmos, 104, 30309-30317, 1999.

Jickells, T. D., Knap, A., Church, T., Galloway, J., and Miller, J.: Acid-Rain on Bermuda, Nature, 297, 55-57, https://doi.org/10.1038/297055a0, 1982.

Kadko, D., and Prospero, J.: Deposition of Be-7 to Bermuda and the regional ocean: Environmental factors affecting estimates of atmospheric flux to the ocean, J Geophys Res-Oceans, 116, C02013, https://doi.org/10.1029/2010JC006629, 2011.

Kassomenos, P., Vardoulakis, S., Borge, R., Lumbreras, J., Papaloukas, C., Karakitsios, S.: Comparison of statistical clustering techniques for the classification of modelled atmospheric trajectories, Theoretical and Applied Climatology 102, 1–12, https://doi.org/10.1007/s00704-009-0233-7, 2010.

Keene, W. C., Moody, J. L., Galloway, J. N., Prospero, J. M., Cooper, O. R., Eckhardt, S., and Maben, J. R.: Long-term trends in aerosol and precipitation composition over the western North Atlantic Ocean at Bermuda, Atmos Chem Phys, 14, 8119-8135, https://doi.org/10.5194/acp-14-8119-2014, 2014.

Kim, Y., Sievering, H., and Boatman, J.: Volume and surface area size distribution, water mass and model fitting of GCE/CASE/WATOX marine aerosols, Global Biogeochem Cy, 4, 165-177, https://doi.org/10.1029/GB004i002p00165, 1990.

Knop, I., Bansmer, S.E., Hahn, V., Voigt, C.: Comparison of different droplet measurement techniques in the Braunschweig Icing Wind Tunnel, Atmospheric Measurement Techniques, 14, 1761–1781, https://doi.org/10.5194/amt-14-1761-2021, 2021.

Lawson, R.P., O'Connor, D., Zmarzly, P., Weaver, K., Baker, B., Mo, Q., Jonsson, H.: The 2D-S (Stereo) Probe: Design and Preliminary Tests of a New Airborne, High-Speed, High-Resolution Particle Imaging Probe, Journal of Atmospheric and Oceanic Technology 23, 1462–1477, https://doi.org/10.1175/jtech1927.1, 2006.

Li, Q., Jacob, D. J., Fairlie, T. D., Liu, H., Martin, R. V., and Yantosca, R. M.: Stratospheric versus pollution influences on ozone at Bermuda: Reconciling past analyses, J. Geophys. Res., 107, 4611, https://doi.org/10.1029/2002JD002138, 2002.

Lin, J. T., and McElroy, M. B.: Impacts of boundary layer mixing on pollutant vertical profiles in the lower troposphere: Implications to satellite remote sensing, Atmos. Environ., 44(14), 1726–1739, https://doi.org/10.1016/j.atmosenv.2010.02.009, 2010.

Lin, S.-J., and Rood, R. B.: Multidimensional Flux-Form Semi-Lagrangian Transport Schemes, Mon Weather Rev, 124, 2046-2070, https://doi.org/10.1175/1520-0493(1996)124<2046:MFFSLT>2.0.CO;2, 1996.

Liu, H., Jacob, D. J., Bey, I. and Yantosca, R. M.: Constraints from ^{210}Pb and ^{7}Be on wet deposition and transport in a global three-dimensional chemical tracer model driven by assimilated meteorological fields, J. Geophys. Res. Atmos., 106(D11), 12109–12128, https://doi.org/10.1029/2000JD900839, 2001.

Luan, Y., Jaeglé, L.: Composite study of aerosol export events from East Asia and North America, Atmospheric Chemistry and Physics, 13, 1221–1242, https://doi.org/10.5194/acp-13-1221-2013, 2013.

Luo, G., Yu, F., and Schwab, J.: Revised treatment of wet scavenging processes dramatically improves GEOS-Chem 12.0.0 simulations of surface nitric acid, nitrate, and ammonium over the United States, Geosci. Model Dev., 12, 3439–3447, https://doi.org/10.5194/gmd-12-3439-2019, 2019.

Matsui, H., Kondo, Y., Moteki, N., Takegawa, N., Sahu, L.K., Zhao, Y., Fuelberg, H.E., Sessions, W.R., Diskin, G., Blake, D.R., Wisthaler, A., Koike, M.: Seasonal variation of the transport of black carbon aerosol from the Asian continent to the Arctic during the ARCTAS aircraft campaign, Journal of Geophysical Research: Atmospheres 116, D05202, https://doi.org/10.1029/2010jd015067, 2011.

Mead, C., Herckes, P., Majestic, B. J., and Anbar, A. D.: Source apportionment of aerosol iron in the marine environment using iron isotope analysis, Geophys Res Lett, 40, 5722-5727, 2013.https://doi.org/10.1002/2013GL057713, 2013.

Merrill, J. T.: Isentropic Air-Flow Probability Analysis, J Geophys Res-Atmos, 99, 25881-25889, 1994. https://doi.org/10.1029/94JD02211, 1994.

Miller, J. M., and Harris, J. M.: The Flow Climatology to Bermuda and Its Implications for Long-Range Transport, Atmos Environ, 19, 409-414, 1985.https://doi.org/10.1016/0004-6981(85)90162-3, 1985.

Milne, P. J., Prados, A. I., Dickerson, R. R., Doddridge, B. G., Riemer, D. D., Zika, R. G., Merrill, J. T., and Moody, J. L.: Nonmethane hydrocarbon mixing ratios in continental outflow air from eastern North America: Export of ozone precursors to Bermuda, J Geophys Res-Atmos, 105, 9981-9990, 2000.https://doi.org/10.1029/1999JD901117, 2000.

Moody, J. L., and Galloway, J. N.: Quantifying the relationship between atmospheric transport and the chemical composition of precipitation on Bermuda, Tellus B: Chemical and Physical Meteorology, 40, 463-479, https://doi.org/10.3402/tellusb.v40i5.16014, 1988.

Moody, J. L., Oltmans, S. J., Levy II, H., and Merrill, J. T.: A transport climatology of tropospheric ozone, Bermuda: 1988–1991, J. Geophys. Res., 100, 7179-7194, 1995.https://doi.org/10.1029/94JD02830, 1995.

Moody, J. L., Keene, W. C., Cooper, O. R., Voss, K. J., Aryal, R., Eckhardt, S., Holben, B., Maben, J. R., Izaguirre, M. A., and Galloway, J. N.: Flow climatology for physicochemical

properties of dichotomous aerosol over the western North Atlantic Ocean at Bermuda, Atmos Chem Phys, 14, 691-717, 2014.https://doi.org/10.5194/acp-14-691-2014, 2014.

Moteki, N., Kondo, Y., Oshima, N., Takegawa, N., Koike, M., Kita, K., Matsui, H., and Kajino, M.: Size dependence of wet removal of black carbon aerosols during transport from the boundary layer to the free troposphere, Geophys Res Lett, 39, L13802, https://doi.org/10.1029/2012GL052034, 2012.

Muhs, D. R., Budahn, J. R., Prospero, J. M., Skipp, G., & Herwitz, S. R.: Soil Genesis on the Island of Bermuda in the Quaternary: The Importance of African Dust Transport and Deposition., Journal of Geophysical Research-Earth Surface, 117, F03025, https://doi.org/10.1029/2012JF002366, 2012.

Nogueira, M.: Inter-comparison of ERA-5, ERA-interim and GPCP rainfall over the last 40 years: Process-based analysis of systematic and random differences, Journal of Hydrology 583, 124632, https://doi.org/10.1016/j.jhydrol.2020.124632, 2020.

Oltmans, S. J., and Levy, H.: Seasonal Cycle of Surface Ozone over the Western North-Atlantic, Nature, 358, 392-394, 1992.https://doi.org/10.1038/358392a0, 1992.

Oshima, N., Kondo, Y., Moteki, N., Takegawa, N., Koike, M., Kita, K., Matsui, H., Kajino, M., Nakamura, H., Jung, J. S., and Kim, Y. J.: Wet removal of black carbon in Asian outflow: Aerosol Radiative Forcing in East Asia (A-FORCE) aircraft campaign, Journal of Geophysical Research: Atmospheres, 117, D03204, https://doi.org/10.1029/2011JD016552, 2012.

Painemal, D., Corral, A. F., Sorooshian, A., Brunke, M. A., Chellappan, S., Afzali Gorooh, V., Ham, S.-H., O'Neill, L., Smith Jr, W. L., Tselioudis, G., Wang, H., Zeng, X., and Zuidema, P.: An Overview of Atmospheric Features Over the Western North Atlantic Ocean and North American East Coast—Part 2: Circulation, Boundary Layer, and Clouds, Journal of Geophysical Research: Atmospheres, 126, e2020JD033423, https://doi.org/10.1029/2020JD033423, 2021.

Park, R.J., Jacob, D.J., Palmer, P.I., Clarke, A.D., Weber, R.J., Zondlo, M.A., Eisele, F.L., Bandy, A.R., Thornton, D.C., Sachse, G.W., Bond, T.C: Export efficiency of black carbon aerosol in continental outflow: Global implications, Journal of Geophysical Research: Atmospheres 110, D11205, https://doi.org/10.1029/2004jd005432, 2005.

Prados, A. I., Dickerson, R. R., Doddridge, B. G., Milne, P. A., Moody, J. L., and Merrill, J. T.: Transport of ozone and pollutants from North America to the North Atlantic Ocean during the 1996 Atmosphere/Ocean Chemistry Experiment (AEROCE) intensive, J Geophys Res-Atmos, 104, 26219-26233, 1999.https://doi.org/10.1029/1999JD900444, 1999.

Quan, J., Liu, Q., Li, X., Gao, Y., Jia, X., Sheng, J., Liu, Y.: Effect of heterogeneous aqueous reactions on the secondary formation of inorganic aerosols during haze events. Atmospheric Environment 122, 306–312, https://doi.org/10.1016/j.atmosenv.2015.09.068, 2015.

Rolph, G., Stein, A., Stunder, B.: Real-time Environmental Applications and Display sYstem: READY, Environmental Modelling & Software 95, 210–228, https://doi.org/10.1016/j.envsoft.2017.06.025, 2017.

Schuster, G. L., Dubovik, O., and Holben, B. N.: Angstrom exponent and bimodal aerosol size distributions, Journal of Geophysical Research: Atmospheres, 111, D07207, https://doi.org/10.1029/2005JD006328, 2006.

Silva, S. J., Ridley, D. A., and Heald, C. L.: Exploring the Constraints on Simulated Aerosol Sources and Transport Across the North Atlantic With Island-Based Sun Photometers, Earth Space Sci, 7, e2020EA001392, https://doi.org/10.1029/2020EA001392, 2020.

Sinnott, R. W.: Virtues of the haversine, Sky and Telescope, Vol.68, No.2, p.159, 1984.

Sorooshian, A., Anderson, B., Bauer, S. E., Braun, R. A., Cairns, B., Crosbie, E., . . . Zuidema, P.: Aerosol–Cloud–Meteorology Interaction Airborne Field Investigations: Using Lessons Learned from the U.S. West Coast in the Design of ACTIVATE Off the U.S. East Coast, Bulletin of the American Meteorological Society, 100(8), 1511-1528, https://doi.org/10.1175/bams-d-18-0100.1, 2019.

Sorooshian, A., Corral, A. F., Braun, R. A., Cairns, B., Crosbie, E., Ferrare, R., . . . Zuidema, P.: Atmospheric Research over the Western North Atlantic Ocean Region and North American East Coast: A Review of Past Work and Challenges Ahead, Journal of Geophysical Research: Atmospheres, 125(6), e2019JD031626, https://doi.org/10.1029/2019JD031626, 2020.

Stein, A.F., Draxler, R.R., Rolph, G.D., Stunder, B.J.B., Cohen, M.D., Ngan, F.: NOAA's HYSPLIT Atmospheric Transport and Dispersion Modeling System. Bulletin of the American Meteorological Society 96, 2059–2077, https://doi.org/10.1175/bams-d-14-00110.1, 2015.

Stohl, A., Wotawa, G., Seibert, P., Kromp-Kolb, H.: Interpolation Errors in Wind Fields as a Function of Spatial and Temporal Resolution and Their Impact on Different Types of Kinematic Trajectories. Journal of Applied Meteorology 34, 2149–2165, https://doi.org/10.1175/1520-0450(1995)034<2149:ieiwfa>2.0.co;2, 1995.

Su, L., Yuan, Z., Fung, J.C.H., Lau, A.K.H.: A comparison of HYSPLIT backward trajectories generated from two GDAS datasets. Science of The Total Environment, 506-507, 527–537, https://doi.org/10.1016/j.scitotenv.2014.11.072, 2015.

Sun, Q., Miao, C., Duan, Q., Ashouri, H., Sorooshian, S., Hsu, K.: A Review of Global Precipitation Data Sets: Data Sources, Estimation, and Intercomparisons. Reviews of Geophysics 56, 79–107, https://doi.org/10.1002/2017rg000574, 2018.

Todd, D. L., Keene, W. C., Moody, J. L., Maring, H., and Galloway, J. N.: Effects of wet deposition on optical properties of the atmosphere over Bermuda and Barbados, J Geophys Res-Atmos, 108, (D3), 4099, https://doi.org/10.1029/2001jd001084, 2003.

Tunved, P., Ström, J., and Krejci, R.: Arctic aerosol life cycle: linking aerosol size distributions observed between 2000 and 2010 with air mass transport and precipitation at Zeppelin station, Ny-Ålesund, Svalbard, Atmos. Chem. Phys., 13, 3643–3660, https://doi.org/10.5194/acp-13-3643-2013, 2013.

US-EPA: Compendium of Methods for the de-termination of inorganic compounds in ambient air, USEPA/625/R-96/010a, United States Environmental Protection Agency, Washington, D.C., 1999.

Veron, A. J., Church, T. M., Patterson, C. C., Erel, Y., and Merrill, J. T.: Continental Origin and Industrial Sources of Trace-Metals in the Northwest Atlantic Troposphere, J Atmos Chem, 14, 339-351, ~~1992.~~https://doi.org/10.1007/BF00115243, 1992.

Wang, Q., Jacob, D. J., Fisher, J. A., Mao, J., Leibensperger, E. M., Carouge, C. C., Le Sager, P., Kondo, Y., Jimenez, J. L., Cubison, M. J., Doherty, S. J., Sager, P. Le, Kondo, Y., Jimenez, J. L., Cubison, M. J., and Doherty, S.J.: Sources of carbonaceous aerosols and deposited black carbon in the Arctic in winter-spring: implications for radiative forcing, Atmos. Chem. Phys., 11(23), 12453–12473, https://doi~~:~~.org/10.5194/acp-11-12453-2011, 2011, 2011.

Wang, Y.Q., Zhang, X.Y., Draxler, R.R.: TrajStat: GIS-based software that uses various trajectory statistical analysis methods to identify potential sources from long-term air pollution measurement data~~.~~, Environmental Modelling & Software, 24, 938–939, https://doi~~:~~.org/10.1016/j.envsoft.2009.01.004, 2009.

Weinstock, B.: Carbon Monoxide: Residence Time in the Atmosphere, 166, 224–225, https://doi.org/10.1126/science.166.3902.224, 1969.

Wesely, M. L.: Parameterization of surface resistances to gaseous dry deposition in regional-scale numerical models, Atmospheric Environment (1967), 23, 1293-1304, https://doi.org/10.1016/0004-6981(89)90153-4, 1989.

Wolff, G. T., Ruthkosky, M. S., Stroup, D. P., Korsog, P. E., Ferman, M. A., Wendel, G. J., and Stedman, D. H.: Measurements of SOx, NOx and Aerosol Species on Bermuda, Atmos Environ, 20, 1229-1239, ~~1986.~~https://doi.org/10.1016/0004-6981(86)90158-7, 1986.

Wu, S., Mickley, L. J., Jacob, D. J., Logan, J. A., Yantosca, R. M. and Rind, D. Why are there large differences between models in global budgets of tropospheric ozone~~?~~?, J. Geophys. Res. Atmos., 112(D5), 1–18, https://doi~~:~~.org/10.1029/2006JD007801, 2007.

Yu, H., Yang, Y., Wang, H., Tan, Q., Chin, M., Levy, R.C., Remer, L.A., Smith, S.J., Yuan, T., Shi, Y.: Interannual variability and trends of combustion aerosol and dust in major continental outflows revealed by MODIS retrievals and CAM5 simulations during 2003–2017, Atmospheric Chemistry and Physics, 20, 139–161, https://doi~~:~~.org/10.5194/acp-20-139-2020, 2020.

Yu, K., Keller, C. A., Jacob, D. J., Molod, A. M., Eastham, S. D. and Long, M. S.: Errors and improvements in the use of archived meteorological data for chemical transport modeling: an analysis using GEOS-Chem v11-01 driven by GEOS-5 meteorology, Geosci. Model Dev., 11, 305–319, https://doi~~:~~.org/10.5194/gmd-2017-125, 2018.

Zhang, B., Liu, H., Crawford, J. H., Chen, G., Fairlie, T. D., Chambers, S., Kang, C.-H., Williams, A. G., Zhang, K., Considine, D. B., Sulprizio, M. P., and Yantosca, R. M.: Simulation of radon-222 with the GEOS-Chem global model: emissions, seasonality, and convective transport, Atmos. Chem. Phys., 21, 1861–1887, https://doi.org/10.5194/acp-21-1861-2021, 2021.